Sensitivity of lumped and semi-distributed hydrological models to 20 gridded precipitation products in a transboundary basin

P. Pacheco Mollinedo, Frédéric Satgé, Marie-Paule Bonnet, Jorge Molina-Carpio, R. Pillco Zolá, Edson Ramírez, Daniel Espinoza-Romero, Renaud Hostache

Sensitivity of lumped and semi-distributed hydrological models to 20 gridded precipitation products in a transboundary basin

Paula L. Pacheco M. [1,2], Frédéric Satgé[1,2], Marie-Paule Bonnet [1,3], Jorge Molina Carpio[2] , Ramiro Pillco[2] , Edson Ramirez[2], Daniel Espinoza[2] , Renaud Hostache[1]

[1] ESPACE-DEV, Université Montpellier, IRD, Université Guyane, Université Réunion, Université Antilles, Université Avignon, CEDEX 05, 34093 Montpellier, France
[2] Universidad Mayor de San Andrés (UMSA), Instituto de Hidráulica e Hidrologia (IHH), Calle 30 Cota Cota, La Paz, Bolivia
[3] Universidade de Brasilia, Centro do desenvolvimento Sustentavél, Campus Darcy, DF, Brasilia, Brasil

Corresponding author: Paula L. Pacheco M.
Address: ESPACE-DEV, 500 Rue Jean François Breton, 34090 Montpellier, France
Email: paula.pacheco-mollinedo@ird.fr

Keywords: Transboundary basin, gridded precipitation, lumped hydrological model, semi-distributed hydrological model, Titicaca basin

ABSTRACT

This study proposes a dual approach to assess 20 Gridded Precipitation Products (GPPs) within a transboundary region with complex topography. GPPs were first compared with observed precipitation to assess their spatio-temporal accuracy. They were then integrated into a lumped (GR4J) and a semi-distributed (MGB-IPH) hydrological model to evaluate their impact on streamflow simulations for three basins. Even if most GPPs effectively captured the dominant north–south precipitation gradient shaped by the Andean topography, the results show significant variations in GPP effectiveness across the considered basins. The most reliable GPPs for streamflow simulation across Katari, Ilave, and Ramis basins are MSWEP, CHIRPS, and MSWEP when considering the lumped GR4J model and SM2Rain_CCI, IMERG_FR, and SM2Rain_CCI when considering the semi-distributed MGB model. This discrepancy among the models shows that GPPs' reliability assessment is sensitive to the model structure and that different conclusions could be made according to the selected model. Our findings show that the GR4j lumped model is barely influenced by precipitation bias due to its buffering capacity. In contrast, the semi-distributed MGB-IPH model is sensitive to precipitation bias in space and time and therefore is more suitable to reveal GPP inconsistencies. Overall, this study not only provides GPP reliability feedback but also new insights on the respective limits and advantages of different assessment

methods (i.e., gauges, lumped and semi-distributed models). These findings support the development of a practical framework for GPP selection according to the forecast use.

1. Introduction

Hydrological models are essential tools for water resources management and play a critical role in shaping water governance strategies, particularly in transboundary basins where shared resources are subject to differing national policies (Ter Horst et al., 2023; Sahu et al., 2023). Developing reliable models in these contexts is especially challenging due to complex landscapes, limited availability of high-quality hydrometeorological data, and the combined effect of policy differences, unequal technical capacity, and the absence of formal data-sharing agreements (Nawaz et al., 2021; IWMI, 2021; Nguyen et al., 2018).

Accurate precipitation data are essential for hydrological modeling, yet mountainous and transboundary regions—such as the Andean Altiplano—often suffer from sparse in situ observations (Satgé et al., 2019; De Moraes Cordeiro & Blanco, 2021). To address these gaps, Gridded Precipitation Products (GPPs)—which combine satellite data, ground-based observations, and reanalysis outputs—have become widely used and continue to evolve through recent advances in remote sensing and artificial intelligence (Sun et al., 2018; Wang et al., 2017; Zubieta et al., 2015; Ter Horst et al., 2023; Gao et al., 2023; Medrano et al., 2023). However, these innovations also introduce new challenges for validation and calibration. Indeed, GPPs' reliability varies considerably across environments due to the sensitivity of the retrieval methods to local climate, topography, land surface emissivity, and land surface temperature contrast (Prat et al., 2021; Nwachukwu et al., 2020; Sun et al., 2018; Prat et al., 2021; Cao et al., 2023; Satgé et al., 2021; Shiru et al., 2025), reinforcing the need for context-specific assessments.

In South America, few studies have systematically evaluated the reliability of GPPs in the Andean region. For instance, significant GPPs underestimation for intense rainfall events (Blacutt et al. 2015), progressive decrease in GPPs estimates' reliability with increasing topographic slope (Satgé et al., 2016), and

lower GPPs performance across the wet than the dry region (Chen et al., 2022) were already reported. Within the broader TDPS (Titicaca Desaguadero Poopó Salar) system, several studies have assessed GPPs' reliability in comparison to gauge observations (Scheel et al., 2011; Quispe et al., 2023; Satgé et al., 2020) and for climate (Torres-Batlló & Martí-Cardona, 2020) and drought trends analysis (Satgé et al., 2017; Satgé et al., 2019). Despite the known challenges, such as highly variable precipitation regimes and the influence of orographic effects, research specific to the Lake Titicaca basin remains limited (e.g., Quispe et al., 2023; Satgé et al., 2019; Medrano et al., 2023). Upon analyzing these studies, it appears that the best GPP can vary significantly from one location to another, not only due to differences in the assessed GPPs but also because of the specific gauge locations used as references, which are influenced by local environmental characteristics.

Given that precipitation is a key input of hydrological models, it is essential to understand GPP's hydrological applicability comprehensively. As of today, most hydrological modelling-based evaluations have predominantly focused on either lumped (e.g., Beck et al., 2017; Jiang, 2019; Raimonet et al.; Maggioni et al., 2013; Li et al., 2023; Andrade et al., 2024; Satgé et al., 2021), distributed (Gebrechorkos et al., 2024) or semi-distributed (Tan et al., 2021; Zubieta et al., 2015; Dembélé et al., 2020) hydrological models. While lumped models are widely used for their simplicity and low data requirements, their aggregated structure limits insights into how GPPs capture spatial precipitation variability (Martel et al., 2020; Nguyen et al., 2023; Kling & Gupta, 2009; Wan et al., 2025). In contrast, semi-distributed models divide a basin into multiple sub-catchments, which allows considering how GPPs capture precipitation spatial variability (Tan et al., 2021). Ideally, combining both modeling approaches (i.e., lumped and semi-distributed) should provide a more robust assessment of GPPs' performance; however, studies that integrate both lumped and semi-distributed models remain scarce. A few exceptions include studies led in Iran (Jahanshahi et al., 2024) and China (Xu et al., 2014) assessing several GPPs reliability for streamflow modeling using both lumped (HBV and Xinanjiang model, respectively) and semi-distributed (SWAT) models. Similarly, GPPs' reliability for streamflow modeling was assessed in China,

considering both lumped (GR4J) and fully distributed (VIC) models (Guan et al., 2020). The evaluation revealed that GPP reliability assessments were sensitive to the hydrological model considered, with performance rankings differing between lumped and semi-distributed models.

The above-mentioned literature highlights the need for further research to comprehensively assess how GPPs influence hydrological simulations under different model structures (lumped and semi-distributed), particularly in the Andean region, where complex hydrological conditions and scarce observational data complicate model evaluations. Moreover, Wan et al. (2025) pointed out that the influence of hydrological model selection on streamflow simulations may be more significant in dry, high-elevation mountainous regions than in wetter, lowland areas, highlighting the importance of considering regional characteristics when assessing GPP performance.

In this context, our study assesses the reliability of 20 GPPs within the Lake Titicaca basin, a high-altitude, transboundary catchment with distinct precipitation gradients, providing an ideal setting to evaluate GPP applicability. For this purpose, GPPs are first assessed using ground-based rainfall observations to evaluate their spatial and temporal accuracy. Next, we integrated them with two hydrological models—a lumped model (GR4J) and a semi-distributed model (MGB-IPH)—to provide insights into the interaction between model structure and precipitation uncertainty. Our study, focused on the South American Altiplano, presents a comprehensive analytical framework applicable to a wide range of GPPs and replicable in other regions of the world.

2. Materials

2.1 Study Area

The Lake Titicaca Basin (57500 km^2) is a key component of the TDPS (Titicaca, Desaguadero River, Lake Poopó, and Coipasa Salt Lake) hydrological system that spans across Peru, Bolivia, and Chile (Fig.1) (Roche et al., 1992). Lake Titicaca is the primary reservoir in a cascading system, where its waters flow through the Desaguadero River into Lake Poopó and, ultimately, the Coipasa Salt Lake. The lake plays a crucial role in

maintaining the water balance and supporting the hydrological connectivity to downstream arid and semi-arid regions (UNESCO, 2003; Satgé et al., 2021; Pillco Zolá et al., 2019; Canedo et al., 2016). With an average water surface area of 8500 km² and a mean depth of 105 m, Lake Titicaca is the largest freshwater lake in South America (Quispe et al., 2023; Pillco Zolá et al., 2019).

The Titicaca Lake basin is characterized by a tropical high-altitude climate with significant seasonal variations. There is a pronounced wet season from December to March, followed by a long dry period from April to November (Zubieta et al., 2021). The climate transitions from humid (around Lake Titicaca in the north of TDPS) to semi-arid (near Lake Poopó) and arid (around Coipasa Salt Lake in the south), reflecting a strong gradient in humidity. Temperatures generally range from 8°C to 10°C annually, dipping to around 4°C in winter and rising to 12°C in summer. Lake Titicaca moderates the local climate, reducing the frequency and intensity of frosts (Canedo et al., 2016; Medrano et al., 2023).

Considering the importance of Lake Titicaca and its basin within the TDPS system, our study initially targets three pilot sub-basins (Katari, Ilave, and Ramis), chosen based on streamflow data availability. The Ramis basin, covering an area of 14866 km², exhibits substantial variability in flow, with a coefficient of variation (Cv) of 1.27. In comparison, the Katari basin, which spans 2519 km², has a narrower flow range but a higher Cv of 2.06. Meanwhile, the Ilave basin, covering 7,720 km², has a broader flow range with a Cv of 1.91.

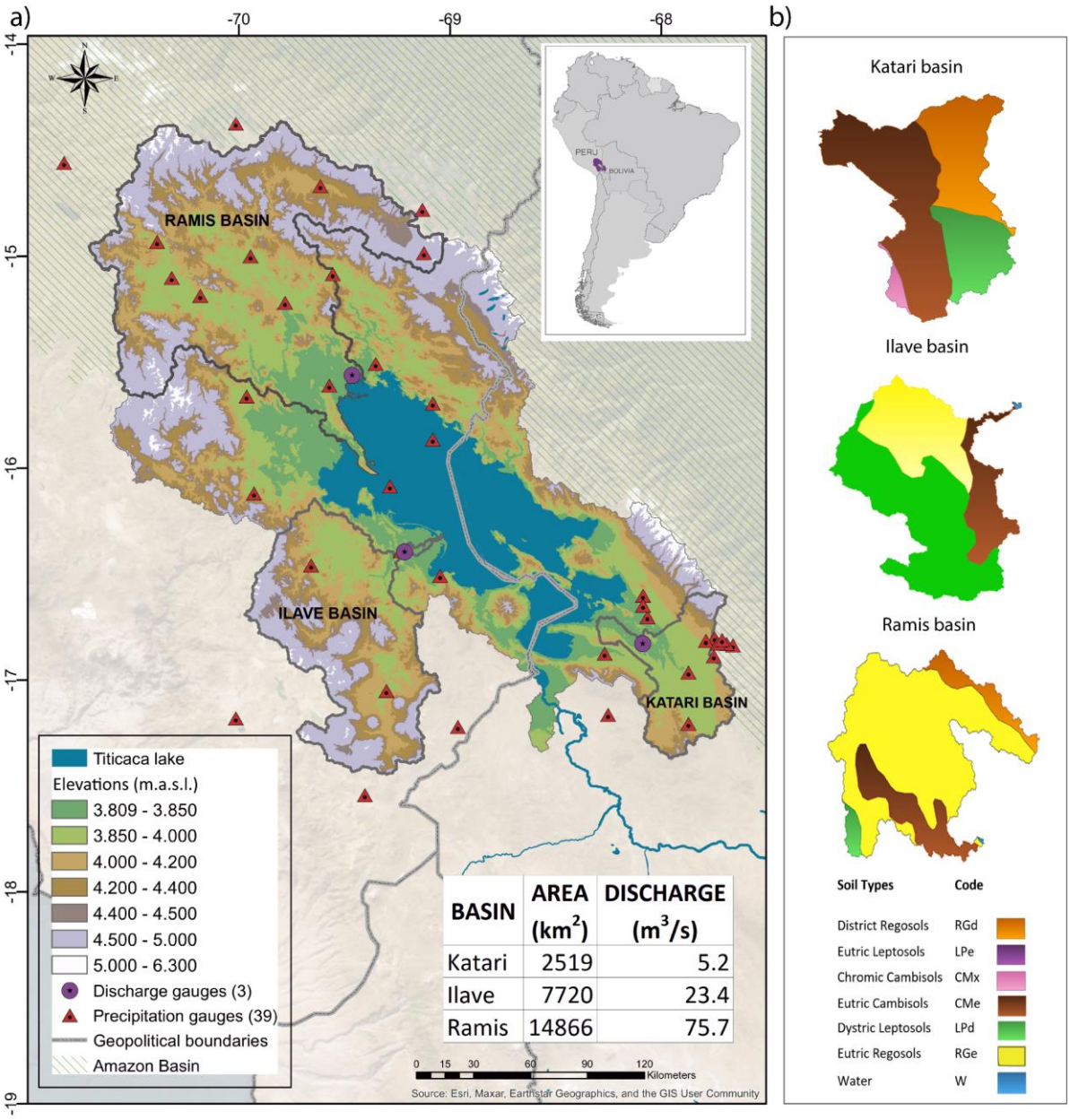

Figure 1 Study area location within (a) TDPS system with the location of precipitation and discharge stations across the three basins along with the South American map indicating the basin's position and the riparian countries, Bolivia and Peru; (b) soil types derived from SOTERLAC.

2.2 Datasets

2.2.1. Digital Elevation Model

With a three arc-second resolution, the MERIT-Hydro Digital Elevation Model (DEM) was used for watershed delineation and drainage network identification. A new algorithm was developed that automatically

identified river networks by distinguishing actual inland basins from artificial depressions often caused by inaccuracies in the input elevation data (Yamazaki et al., 2019).

2.2.2. Land Use Land Cover

This study utilized a MODIS satellite-derived Land Cover Type product (MODIS/Terra+Aqua Land Cover Type Yearly L3 Global 500 m SIN Grid, MCD12Q1). This product has a yearly temporal resolution and 500 m spatial resolution with global coverage, and its performance is well-documented (Friedl & Sulla-Menashe, 2022). The year 2007 was chosen as it falls within the study period from 2002 to 2015 to ensure a fair representation of the basin's land use and land cover state.

2.2.3. Soil data

Soil information was obtained from the soils and terrains for Latin America and the Caribbean version 2 (SOTERLAC v.2) (Dijkshoorn et al., 2005). Using the FAO soil classification system, SOTERLAC was constructed by compiling and harmonizing soil and terrain data from various national sources in Latin America and the Caribbean, digitized at a 1:5 million scale resolution and validated through field verification and expert reviews for accuracy. Fig. 1 shows the three subbasins' soil maps.

2.2.4. Evapotranspiration

Climate data, including temperature, humidity, wind speed, sunshine hours, and atmospheric pressure, were sourced from the ERA5 reanalysis dataset for the period 2002-2015. ERA5, provided by ECMWF (European Centre for Medium-Range Weather Forecasts), delivers hourly data with global coverage and a spatial resolution of 0.25° x 0.25° (Hersbach et al., 2020). This climate data was processed using Python and later integrated into the MGB model (Modelo Hidrológico de Grandes Bacias, hereafter referred to as MGB) to compute the potential evapotranspiration using the Penman-Monteith equation (Collischonn et al., 2007; De Paiva et al., 2013; Allen & Food and Agriculture Organization of the United Nations, 1998).

2.2.5. Observed precipitation and discharge

The Servicio Nacional de Meteorología e Hidrología (SENAMHI) in Bolivia and Peru provided observed daily precipitation data for the period 2002-2015. A buffer was applied around each basin to ensure comprehensive spatial coverage, obtaining data from 39 stations in the three basins (Figure 1). Daily discharge measurements for the same period were obtained from the National Water Authority (ANA) in Peru and SENAMHI in Bolivia for each of the three basins.

2.2.6. Gridded precipitation products

Several GPPs have been developed in recent decades to meet the needs of hydrological analysis. These datasets utilize satellite observations, gauge measurements, atmospheric model simulations, or a combination of them (e.g., reanalysis products; see Table 1). Twenty specific gridded precipitation products were selected for this study as they provide extensive spatial coverage, high temporal resolution, and advanced integration methods.

The selected GPPs encompass various iterations of similar precipitation products, each differing in resolution and data correction levels. These versions range from primarily satellite-based to those enhanced with local observational corrections. Additionally, each version is tailored to meet different analytical needs due to its unique characteristics and availability timelines, ensuring that they serve distinct purposes within our hydrological analysis.

Table 1 Overview of the GPP adopted in this study. The Abbreviations: "R" stands for Reanalysis, "G" for Gauge, and "S" for satellite

Short name	Full name	Data source	Temporal coverage	Temporal resolution	Spatial coverage	Spatial resolution	References
CHIRP v.2	Climate Hazard Group InfraRed Precipitation	SR	1981–present	Daily	Global (LAND)	0.05°	(Funk et al., 2015)
CHIRPS v.2	Climate Hazard Group InfraRed Precipitation with Stations	SRG	1981–present	Daily	50°S to 50°N	0.05°	(Funk et al., 2015)
CMORPH_BLD	Bias-Corrected CMORPH Further Blended with Gauge Analysis	SG	1998–present	Daily	60°S to 60°N	0.25°	(Joyce et al., 2004)
CMORPH_CRT	CPC MORPHing technique (CMORPH) bias-corrected (CRT) V1.0	SG	1998-2015	Hourly	60°S to 60°N	0.25°	(Joyce et al., 2004)
ERA5	ERA5: Fifth Generation of ECMWF Atmospheric Reanalyses of the Global Climate	R	1979–present	Hourly	Global	0.25°	(Hersbach et al., 2020)
GSMaP_Adj v.6	Global Satellite Mapping of Precipitation-adjusted	SG	2000-present	Hourly	60°S to 60°N	0.1°	(Ushio et al., 2009; Kubota et al., 2020)
GSMaP_RT v.6	Global Satellite Mapping of Precipitation Standard	S	2000-present	Hourly	60°S to 60°N	0.1°	(Ushio et al., 2009;

							Kubota et al., 2020)
IMERG-ER v.6	Integrated Multi-satellitE Retrievals for GPM-IMERG–Early run v.6	S	2000–present	30 min	Global	0.1°	(Huffman et al., 2020)
IMERG-FR v. 6	Integrated Multi-satellitE Retrievals for GPM-IMERG–Final run v.6	SG	2000–present	30 min	Global	0.1°	(Huffman et al., 2020)
IMERG-LR v. 6	Integrated Multi-satellitE Retrievals for GPM-IMERG–Late run v.6	S	2000–present	30 min	Global	0.1°	(Huffman et al., 2020)
MERRA2_Flx	Modern-Era Retrospective Analysis for Research and Applications, Version 2 (MERRA-2) - Flux Precipitation Total	R	1980-present	hourly	Global	0.5°	(Gelaro et al., 2017)
MERRA2_LND	MERRA-2 Land Precipitation Total Correction	RG	1980–present	hourly	Global	0.5°	(Gelaro et al., 2017)
MSWEP v.2.8	Multi-Source Weighted Ensemble Precipitation v.2.8	SRG	1979–present	3 hr	Global	0.1°	(Beck et al., 2019)
PERSIANN_CDR	Precipitation Estimation from Remotely Sensed Information using Artificial Neural Networks - Climate Data Record	SG	1983-present	daily	60°S to 60°N	0.25°	(Ashouri et al., 2015)
PERSIANN_CSS_CDR	Precipitation Estimation from Remotely Sensed Information using Artificial Neural Networks-Cloud Classification System-Climate Data Record	SG	1983-present	3-hourly	60°S to 60°N	0.04°	(Sadeghi et al., 2021)
SM2Rain_CCI v.2	Soil Moisture to Rain from ESA Climate Change Initiative	S	1998–2021	Daily	Global (LAND)	0.1°	(Mosaffa et al., 2023)
TMPA_Adj	Tropical Rainfall Measuring Mission Multi-Satellite Precipitation Analysis - Adjusted	SG	1998-2019	2 hours	60°S to 60°N	0.25°	(Huffman et al., 2010; Huffman et al., 2018)
TMPA_RT	Tropical Rainfall Measuring Mission Multi-Satellite Precipitation Analysis - Real Time	S	2000-2019	3 hours	60°S to 60°N	0.25°	(Huffman et al., 2010; Huffman et al., 2018)
WFDEI_CRU	WATCH Forcing Data methodology applied to ERA-Interim data with CRU corrections	RG	1979-2015	Daily	Global	0.5°	(Weedon et al., 2014)
WFDEI_GPCC	WFDEI c2017 0.5 x 0.5-degree global meteorological forcing data	RG	1976-2016	Daily	Global	0.5°	(Weedon et al., 2018)

2.3 Hydrological Models

2.3.1 MGB-IPH model

MGB is a semi-distributed model developed by the Federal University of Rio Grande do Sul and tailored for large-scale basins. It uses a combination of physical and conceptual equations to simulate key hydrological processes, including infiltration, evapotranspiration, runoff, and river flow (Collischonn et al., 2007; Collischonn & Tucci, 2001). The model divides basins into smaller catchments, each with specific hydrological balances (Siqueira et al., 2018).

Hydrological Response Units (HRUs) are defined based on combinations of soil types and land use (Haghnegahdar et al., 2015). Water and energy budgets for each HRU are calculated using a simplified reservoir model for soil (De Paiva et al., 2013) and the Penman-Monteith equation for evapotranspiration (Allen & FAO, 1998). Runoff and groundwater flows are routed using various methods, including linear reservoirs and hillslope routing (Todini, 1996). The Muskingum-Cunge equation is used to simulate water propagation within the drainage system. The model has been widely employed in watersheds exceeding 2,500 km^2 in South America and Africa (Fleischmann et al., 2017) and has been used in studies aiming at modeling the Amazon River basin and assessing climate change impacts (Paiva et al., 2011; Paiva et al., 2013; Siqueira et al., 2018; Brêda et al., 2020).

Table 2 lists the soil parameters used for calibration, including Wm and b, which Oliveira et al. (2019) identified as the most sensitive. These parameters significantly influence the simulation of maximum and minimum streamflows and overall model bias (Collischonn et al., 2007).

Table 2 MGB model parameters

Parameter	Units	Limits [min-max]	Description
Wm	mm	[50 – 1000]	Soil moisture capacity (the capacity of the soil to store rainwater, generating little or no runoff)
b	-	[0.01 – 1.6]	Defines the shape of the storage-saturation curve (controls the separation of runoff to saturation of the soil storage capacity)
Kbas	days	[0.05 – 5]	Controls flow during dry periods; affects baseflow generation
Kint	-	[4 – 40]	Amount of soil water that emerges as subsurface flow
CAP	mm/day	[0]	Flow rate from the subsurface reservoir to the surface soil layer
Wc	mm	[0.1–0.825×Wm]	Residual storage limits the flow of sub-surface and underground water
CS	-	[1-20]	Coefficient for surface water propagation in cells
CI	-	[50-200]	Coefficient for sub-surface water propagation in cells
CB	days	[1200 – 8000]	Delay parameter of the underground reservoir

2.3.2 GR4J Model

GR4J (Génie Rural à 4 paramètres Journalier) is a conceptual rainfall-runoff model developed in France (Perrin et al., 2003). It uses four parameters to simulate the hydrological cycle based on daily precipitation and potential evapotranspiration (PET) (Table 3). The model employs two reservoirs and two-unit hydrographs to convert rainfall into runoff, with adequate precipitation accounting for daily PET.

The GR4J model was selected for this study due to its proven reliability in a wide range of regions, including Europe (Fabre et al., 2015), Asia and Oceania (Wei et al., 2021), and Africa (Kodja et al., 2020; Faty et al., 2023; Ndiaye et al., 2024). In South America, the model has been applied with success in Chile (Ruelland et al., 2014; Hublart et al., 2015, 2016), Brazil (Satgé et al., 2021), Ecuador (Pozo Valdivieso, 2024), and across the Titicaca region (Satgé et al., 2019).

Table 3 GR4J model parameters

Parameter	Units	Limits [min-max]	Description
X_1	mm	[100-2000]	Maximum capacity of the production store
X_2	mm/day	[-5 - 3]	Groundwater exchange coefficient
X_3	mm	[20 – 300]	Maximum capacity of the routing store
X_4	days	[1.1 - 2.9]	Base time of the unit hydrograph

3. Methodology

3.1 Hydrological Modeling Set-up and Calibration

The three basins (Katari, Ilave, and Ramis) were delineated using IPH-Tools in QGIS. This tool utilizes a series of geoprocessing algorithms to (i) fill and remove depressions (sinks), (ii) calculate flow direction based on terrain slope, (iii) compute flow accumulation by determining the upstream contributing area, and (iv) delineate drainage areas and sub-basins. These steps resulted in a detailed drainage network segmented into micro-basins, forming the larger basin structure (Siqueira et al., 2016). Additional processing included stream ordering and thresholding to define the river network, ensuring accurate hydrological representation.

For the MGB model, HRUs were defined by integrating land cover data from MODIS and soil data from SOTERLAC using IPH-Tools. Essential baseline data for each HRU were stored in the MINI.gtp file and facilitated the modeling of localized hydrological processes within each sub-basin (Pontes et al., 2017). Potential Evapotranspiration (PET) was computed in MGB from ERA5 climate variables. Then, observed and GPP data were interpolated at the sub-basin level using Python scripts and formatted for the MGB model. Finally, Monte Carlo simulations were used to calibrate MGB for each of the products following a four-step process (Hostache et al., 2020):

1. Generate 10,000 MGB parameter sets using hypercube sampling

2. Run 10,000 MGB simulations using each of the previously generated parameter sets
3. Compute the KGE for each MGB simulation
4. Select the optimal parameter set providing the highest KGE value.

In the GR4J model, PET, derived from the MGB model outputs and observed, and GPP data were aggregated at the basin scale. Then, the open-source Modular Assessment of Rainfall-Runoff Models Toolbox v.1.2 (Knoben et al., 2019) was used to set up the model with the Nelder–Mead simplex algorithm for the objective function optimization (KGE) to calibrate it. The model was recalibrated independently for each GPP to tailor the model parameters to the unique characteristics of each precipitation dataset.

For both models (MGB and GR4J), a model warm-up was performed from 2002 to 2004, and the calibration was carried out from 2005 to 2012. The same calibration method was applied consistently for each GPP and basin, following a standardized approach across the dataset. Recent studies have adopted similar methodologies, such as Andrade et al. (2024), who utilized a uniform calibration strategy across multiple precipitation products to ensure comparability and robust model performance across diverse hydrological conditions.

3.2. GPPs accuracy assessment

3.2.1 Spatial Pattern Assessment

Annual-averaged precipitation maps for the 2002–2015 period were generated at a regional level for all 20 GPPs using downloaded daily data. The maps cover a quadrant that includes the three basins under study. These data were then mapped onto their original grids, maintaining the native resolution of each product to ensure consistency. This approach allows a clearer understanding of how differences in resolution may impact the spatial representation of precipitation patterns.

Observation Gauges were strategically selected within a rectangular area that encompasses each basin, extending 10 to 30 km beyond their boundaries to ensure the inclusion of relevant and reliable station data. Additionally, stations from the Amazon basin were included as reference points, allowing for a clearer

representation of the regional precipitation gradient. Furthermore, the annual average precipitation for each station was calculated based on the available daily data. These values were then mapped using a color scale ranging from 0 to 2000 mm/year, similar to those used for the GPPs. Finally, the resulting 21 maps were visually assessed to analyse the spatial distribution of precipitation and its alignment with expected regional climatic patterns.

3.2.2 Temporal Accuracy Analysis

To ensure a uniform data distribution across the study area, the 20 GPPs and gauge observations were interpolated using the sub-basin discretization approach of the MGB model (Figure 2). In MGB, the watershed is divided into sub-units called minibasins, which correspond to immediate contribution areas to a river segment and are delineated based on digital elevation models and geoprocessing algorithms. We have applied the inverse distance weighting method, assigning values to the centroid of each minibasin. This approach allows for a more accurate representation of the spatial heterogeneity of physical characteristics and hydrological fluxes within the watershed. The interpolated precipitation in each mini-basin was subsequently used for statistical analyses, ensuring a more consistent comparison between different precipitation products.

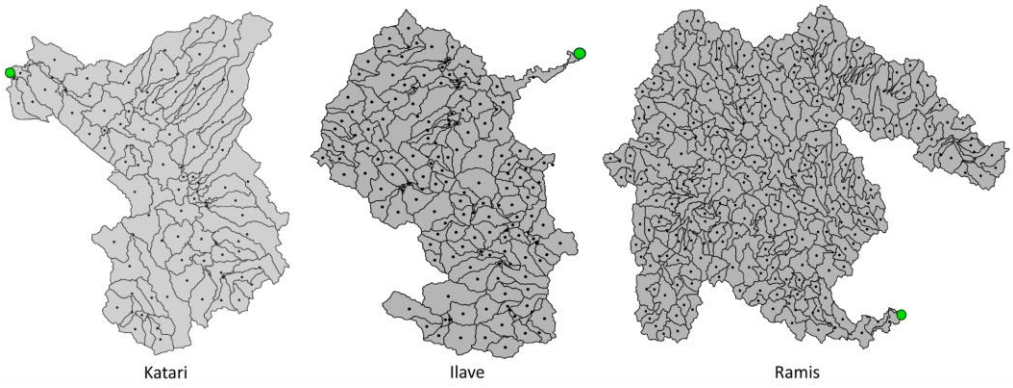

Figure 2 Minibasins with their corresponding centroids, and in green, the outlets of each basin

Following the described process, the temporal accuracy of the GPPs was assessed by comparing the spatially averaged GPP values to the spatially averaged gauge observations at a daily time step. Taylor diagrams (Taylor, 2001) were used to visualize this comparison based on three key metrics:

- Correlation (R, Eq. 1): Measures the strength and direction of the linear relationship between observed and GPP values, represented by the angular position in the Taylor diagram.
- Standard Deviation (σ, Eq. 2): Reflects the variability of the dataset around its mean.
- Centered Root-Mean-Square Difference (CRMSD, Eq. 3): Evaluates discrepancies between observed and GPP patterns, focusing on differences in spatial or temporal structures.

Bias (Eq. 4) was also calculated to quantify systematic estimation errors.

$$R = \frac{1}{N-1}\sum_{i=1}^{N}\left(\frac{X_i - \overline{X}}{\sigma X}\right)\left(\frac{Y_i - \overline{Y}}{\sigma Y}\right) \quad (1)$$

$$\sigma = \sqrt{\frac{1}{N}\sum_{i=1}^{N}(X_i - \overline{X})^2} \quad (2)$$

$$CRMSD = \sqrt{\frac{1}{N}\sum_{i=1}^{N}(X_i - \overline{X} - Y_i - \overline{Y})^2} \quad (3)$$

$$Bias\ (\%) = \left(\frac{\sum(Yi - Xi)}{\sum Xi}\right) * 100 \quad (4)$$

Where X_i and Y_i represent the observed and simulated values, respectively, $\overline{X}$ and $\overline{Y}$ are the means of the observed and GPPs values, σX and σY are the standard deviations of the observed and GPPs values *and* N is the number of observations.

.

3.3 GPPs as input precipitation data within Hydrological Models

For each Gridded Precipitation Product (GPP) and model (MGB and GR4J), streamflow simulations were conducted across the three basins for the calibration period: 2005-2012. To assess the reliability of the simulated streamflow, KGE values were computed for this period (Eq. 5), focusing on evaluating model performance rather than optimizing it for predictive purposes, as evaluating the validation period could

introduce additional sources of uncertainty. In recent years, KGE has been extensively employed to calibrate and evaluate hydrological models (Liu, 2020). The application of KGE within the context of this study is justified by its ability to provide nuanced insights into the model's behavior, providing a more balanced assessment of model errors compared to the Nash-Sutcliffe Efficiency (NSE) (Gupta et al., 2009). The KGE values range from negative infinity to one, with a value of one representing perfect agreement and negative values indicating poor performance.

$$KGE = 1 - \sqrt{(R-1)^2 + (\alpha-1)^2 + (\beta-1)^2} \quad (5)$$

Where R is the Correlation coefficient between the observed X_i and simulated Y_i values. α is the ratio of the means (*Eq. 6*), and β is the ratio of the coefficients of variation (*Eq. 7*)

$$\alpha = \frac{\overline{Y}}{\overline{X}} \quad (6)$$

$$\beta = \frac{\sigma Y/\overline{Y}}{\sigma X/\overline{X}} \quad (7)$$

4. Results

4.1. GPPs Spatial Pattern Assessment

Figure 3 presents the annual-averaged precipitation maps for the 2002–2015 period for all 20 GPPs, preserving their native resolutions (Table 1). The figure also includes observation gauges. The assessment reveals notable differences in how each dataset represents spatial precipitation patterns across the study area, highlighting variations in resolution, consistency, and potential outliers.

The area of interest represented in Figure 3 not only covers the Titicaca basin but also extends into a portion of the Amazon Basin, which experiences markedly higher precipitation levels (Molina-Carpio et al., 2023). This broader regional analysis captures the transition between the humid north-eastern areas, influenced by Amazonian rainfall patterns, and the drier south-western regions. In that sense, a transparent precipitation

gradient is observed across the region, reflecting the described gradient captured by most of the products; however, differences in resolution and absolute precipitation values lead to varying degrees of agreement.

Some GPPs, such as CHIRPS, GSMaP_RT, IMERG-FR, MSWEP, TMPA_Adj, and WFDEI_CRU, align more closely with the expected precipitation distribution. The observation stations in Figure 3 provide additional context, notably confirming the transition from humid to drier zones influenced by the Amazon. Some products like CHIRPS and IMERG-FR capture this feature more effectively.

On the other hand, ERA5 and MERRA2_FLX exhibit a significant overestimation of precipitation across the entire domain, deviating considerably from other datasets. Regarding SM2RAIN_CCI, although its coverage is limited in some areas, where data is available, it follows the typical precipitation pattern observed across multiple products.

When considering spatial resolution, a higher resolution does not always lead to a better representation of precipitation gradients. For example, TMPA_Adj, WFDEI_CRU, and WFDEI_GPCC, despite having coarser resolutions, appear to represent precipitation distribution well. In contrast, PERSIANN_CSS_CDR, despite having the highest resolution among all GPPs, does not align with the general trend observed across most products, suggesting a potential overestimation.

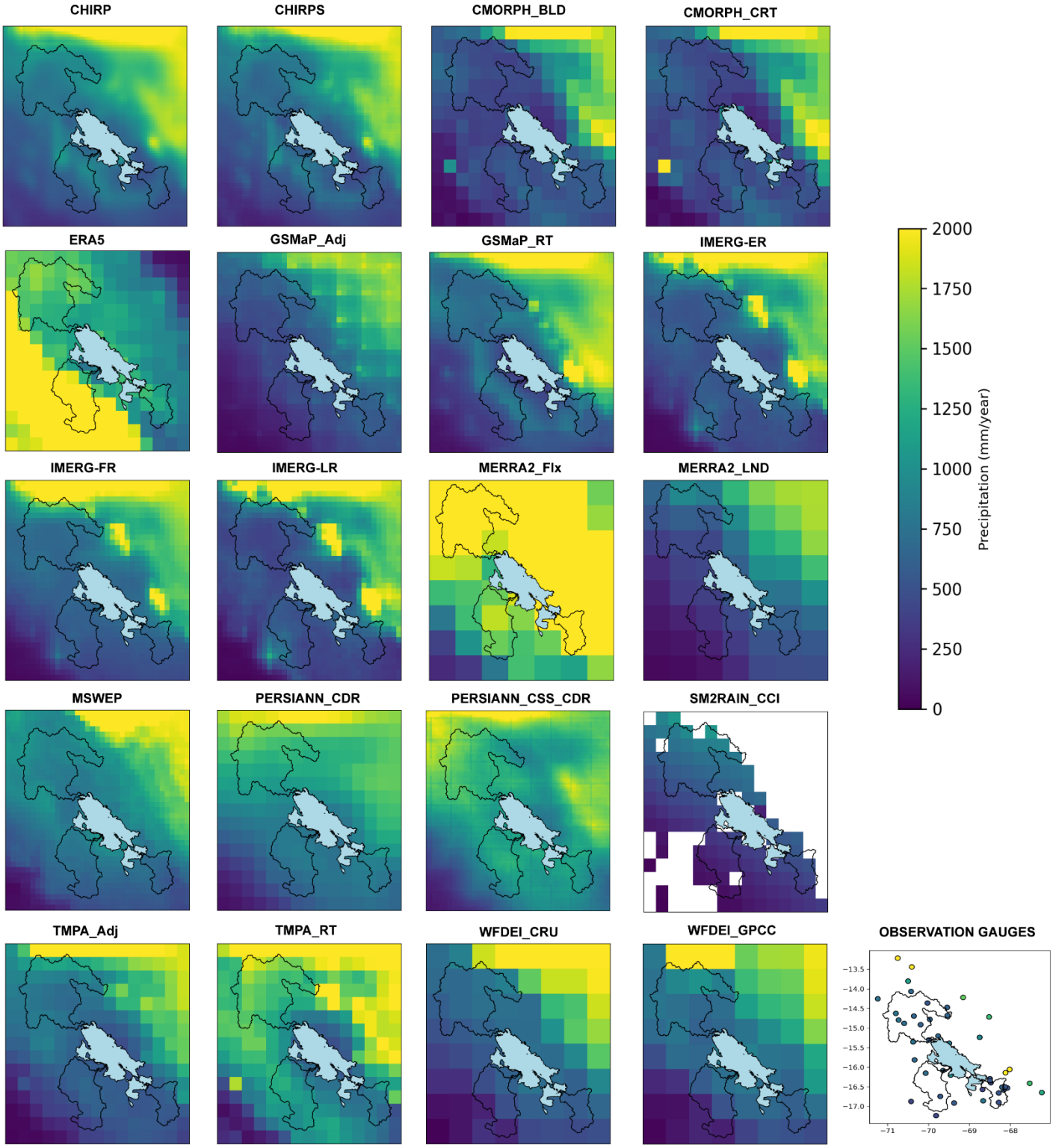

Figure 3 Annual average precipitation maps derived from the 20 GPPs and gauge observations for the 2002-2015 period.

4.2.GPPs' temporal reliability

Key statistical metrics were computed to assess the temporal reliability of the GPPs in the Katari, Ilave, and Ramis basins. These indicators provide insights into each GPP's ability to replicate observed precipitation patterns in terms of variability, agreement with observations, and systematic deviations. Table 4 presents the statistical evaluation of each product for the three basins.

Table 4 Statistical indicators for the evaluation of GPPs' temporal performance in the three basins (Katari, Ilave, Ramis).

Basin	Product	STDs	CRMSD	CCOEF	Bias	Basin	STDs	CRMSD	CCOEF	Bias	Basin	STDs	CRMSD	CCOEF	Bias
KATARI	CHIRP	1.10	0.59	0.84	6	ILAVE	0.97	0.51	0.87	18	RAMIS	1.16	0.46	0.92	26
	CHIRPS	1.05	0.54	0.86	-2		0.88	0.43	0.90	4		1.02	0.43	0.91	9
	CMORPH_BL	1.09	0.62	0.83	5		0.61	0.60	0.83	-19		0.65	0.53	0.88	-32
	CMORPH_CRT	0.91	0.57	0.82	-11		0.60	0.59	0.85	-18		0.67	0.49	0.90	-29
	ERA5	2.66	2.09	0.69	301		1.28	0.51	0.93	86		1.31	0.60	0.90	56
	GSMaP	1.08	0.61	0.83	6		0.70	0.64	0.77	-40		1.00	0.75	0.72	-22
	GSMaP_RT	1.07	0.71	0.77	22		0.80	0.64	0.77	0		0.84	0.54	0.84	3
	IMERG-ER	1.07	0.54	0.87	10		0.83	0.37	0.93	-13		0.76	0.43	0.92	-8
	IMERG-FR	1.17	0.55	0.88	16		0.92	0.34	0.94	-10		1.08	0.35	0.94	21
	IMERG-LR	1.08	0.53	0.87	3		0.84	0.36	0.94	-16		0.70	0.43	0.93	-20
	MERRA2_FLX	3.44	2.87	0.67	430		1.90	1.08	0.91	155		3.10	2.44	0.75	503
	MERRA2_LND	1.02	0.39	0.93	5		0.50	0.59	0.90	-51		0.79	0.50	0.87	-19
	MSWEP	1.14	0.43	0.93	20		1.17	0.38	0.95	15		1.28	0.42	0.96	32
	PERSIANN_CDR	1.33	0.70	0.86	56		8.80	8.76	0.25	-424		1.46	0.69	0.91	85
	PERSIANN_CSS_CDR	1.61	1.03	0.78	93		1.44	0.69	0.90	76		1.48	0.76	0.88	94
	SM2Rain_CCI	0.84	0.50	0.87	-23		0.40	0.67	0.89	-75		1.07	0.43	0.92	1
	TMPA_Adj	1.02	0.59	0.83	5		0.89	0.41	0.91	-7		1.05	0.44	0.91	19
	TMPA_RT	1.31	0.81	0.79	42		1.25	0.62	0.87	64		1.66	0.92	0.87	106
	WFDEI_CRU	1.09	0.58	0.85	7		0.87	0.43	0.90	-24		1.10	0.42	0.92	2
	WFDEI_GPCC	1.06	0.55	0.86	13		0.90	0.40	0.92	-14		1.07	0.39	0.93	16

To better understand the performance of the GPPs in capturing precipitation variability, we use a Taylor diagram, which provides a comprehensive visualization of key statistical metrics (Figure 4). This approach allows for an integrated assessment of correlation, variability, and centered root mean square deviation (CRMSD), facilitating a direct comparison across datasets. Additionally, a bias bar graph is included to highlight systematic deviations from observed precipitation, offering further insight into the tendencies of each product in the three basins. Figure 4 presents these results, summarizing the statistical performance of the GPPs.

The Taylor diagram reveals notable differences in the performance of GPPs across the three basins. Overall, CHIRPS, IMERG-FR, and MSWEP exhibit the highest correlation coefficients (CCOEF > 0.90) across all basins, indicating strong agreement with the reference dataset. In contrast, products such as GSMaP_Adj and MERRA2_FLX display significantly lower correlation values (CCOEF < 0.75), with PERSIANN_CDR

showing particularly high CRMSD values mainly in the Ilave basin, suggesting substantial errors in capturing the temporal variability of precipitation. Due to the extreme values of standard deviation (STD) or CRMSD, some products were removed from the Taylor diagrams for clarity: ERA5 and MERRA2_FLX in the Katari basin, PERSIANN_CDR in the Ilave basin, and MERRA2_FLX in the Ramis basin.

Regarding bias, MERRA2_FLX, PERSIANN_CDR, and ERA5 present the most pronounced absolute bias in the three basins. In comparison, CHIRPS and IMERG-ER show relatively low bias values across the three basins. A basin-specific bias analysis highlights that the Ilave basin generally exhibits the lowest bias among GPPs, with most products displaying values within ±50%. Among the analyzed products, GSMaP_RT stands out due to its low bias across all basins. Notably, in the Ilave basin, GSMaP_RT presents a bias of 0%, indicating an almost perfect agreement in magnitude. It is important to note that, due to the scale used in the bias plot (ranging from -100% to 100%), products that exceeded this range were still plotted, but their bias values were displayed in white text on the bars.

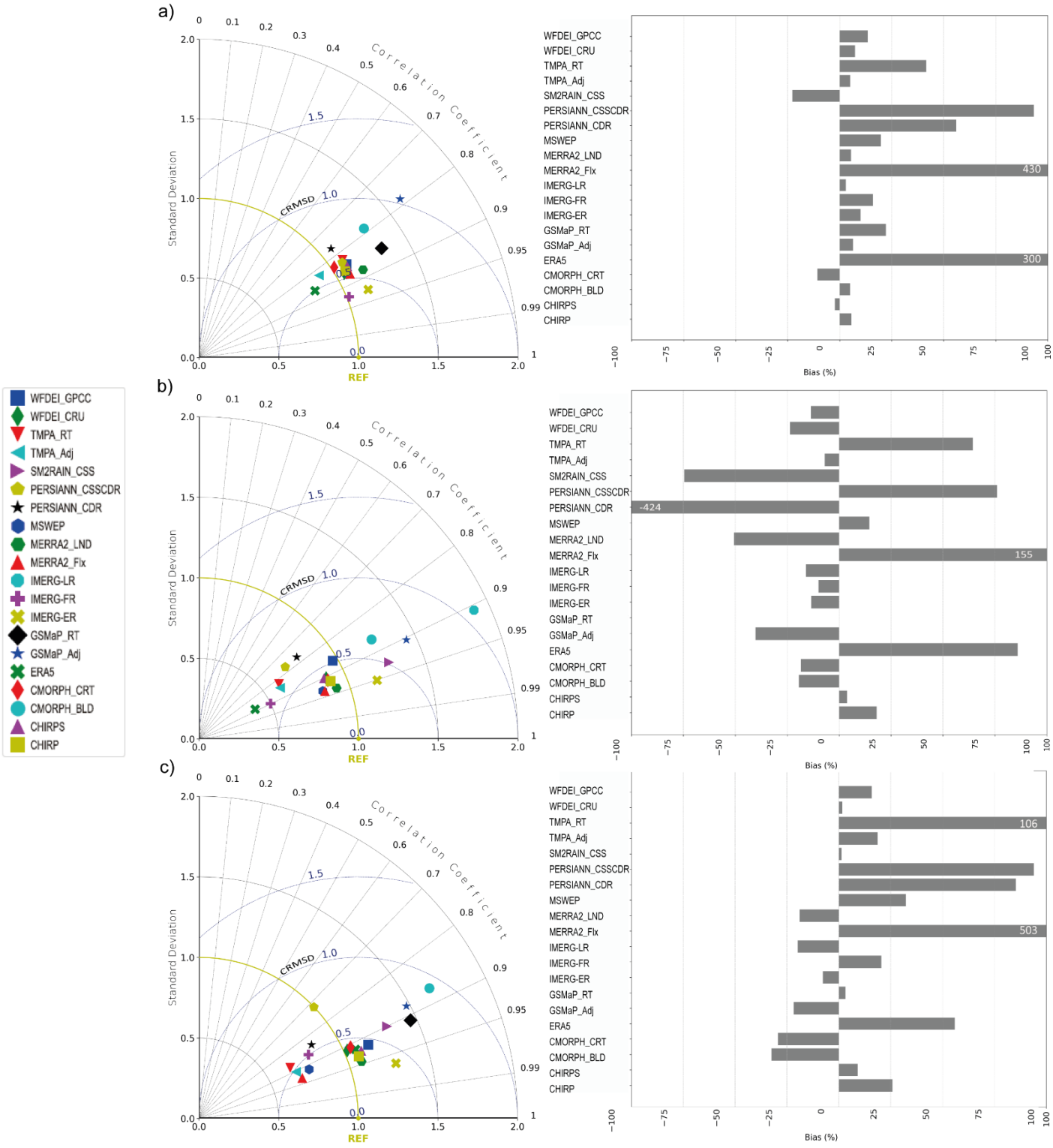

Figure 4 Taylor diagrams (left column) and bias bar charts (right column) comparing the different precipitation datasets for the (a) Katari, (b) Ilave, and (c) Ramis basins (one row for each basin). In the Taylor diagrams, precipitation datasets with a standard deviation beyond the plot range were excluded (Katari->MERRA2_Flx, Ilave->PERSIANN_CDR, Ramis-> MERRA2_Flx). Adjacent to each Taylor diagram, a bar chart shows the bias calculation for each dataset, plotted within the range of -100 % to 100%. Bars exceeding this range are marked with their respective bias percentage inside the bar.

4.3. Hydrological Model Performance Sensitivity to GPPs

The impact of the GPPs on the performance of both models was assessed by comparing streamflow simulations using these products as input in Figure 5. For each GPP, distinct parameter sets were calibrated to optimize the model's responses to the characteristics of precipitation data.

In the Katari basin, GR4J showed high performance, while MGB had moderate performance represented by KGE with CHIRPS (0.84, 0.70), MSWEP (0.88, 0.68), and IMERG_FR (0.83, 0.58), respectively. In contrast, SM2Rain_CCI led to good performance in MGB (0.77) but had a weaker influence on GR4J (0.49), suggesting its robustness in semi-distributed simulations. Finally, PERSIANN_CSS_CDR, MERRA2_FLX, and ERA5 resulted in poor performance in both models (KGE < 0.50).

In the Ilave basin, the GR4J and MGB models both achieved high performance, as reflected by KGE values, with IMERG_FR (0.83, 0.86), IMERG_LR (0.83, 0.81), and CHIRPS (0.85, 0.82), demonstrating their consistency across models. In contrast, some GPPs showed strong performance in GR4J but were less effective in MGB, such as GSMaP_Adj (0.73, 0.49), ERA5 (0.73, <0), and MERRA2_LND (0.72, 0.45), suggesting a model-dependent sensitivity to precipitation inputs. Conversely, WFDEI_CRU contributed to good performance in MGB (KGE = 0.74) but failed to adequately support GR4J (KGE = 0.31). Finally, SM2Rain_CCI and GSMaP_RT resulted in poor performance in both models (KGE < 0.50).

The evaluation of GPPs in the Ramis basin shows a clear differentiation between datasets that perform consistently well across hydrological models and those with model-dependent effectiveness. SM2Rain_CCI (0.83, 0.90), IMERG_LR (0.84, 0.82), and CHIRPS (0.90, 0.79) demonstrated high performance in both GR4J and MGB. Meanwhile, MSWEP (0.93, 0.59) showed very high performance in GR4J but only regular performance in MGB, while ERA5 (0.84, <0) and PERSIANN_CDR (0.82, <0) also exhibited strong results in GR4J but were ineffective in MGB. On the other hand, GSMaP_Adj (0.12, 0.48) and MERRA_FLX (0.45, <0) yielded poor performance in both models, indicating their limited applicability for hydrological modeling in the Ramis basin.

In summary, CHIRPS and IMERG products showed consistently strong performance across both hydrological models, achieving high skills in all basins. In contrast, MSWEP performed well in all basins with the lumped GR4J model, while ERA5 showed good performance only in the Ilave and Ramis basins. However, both products exhibited substantially lower performance in the semi-distributed MGB model. Conversely, SM2Rain_CCI (in Katari) and WFDEI_CRU (in Ilave) yielded better results with MGB than with GR4J, highlighting the influence of model structure. Finally, PERSIANN_CSS_CDR and MERRA2_FLX consistently exhibited low performance in both models (KGE < 0.50), indicating limited suitability for streamflow simulation in this context.

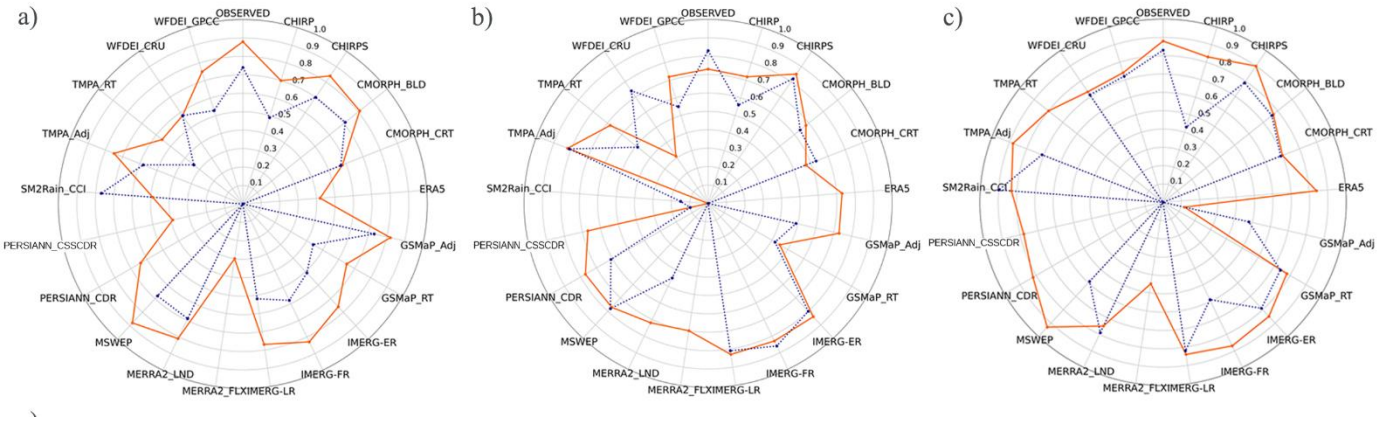

Figure 5 Radar charts showing KGE results for both hydrological models in the Katari (a), Ilave (b), and Ramis (c) basins. The simulation with MGB is represented in a blue dashed line, while the simulation with GR4J is shown in an orange solid line.

Figure 6 shows streamflow hydrographs simulated for the Katari, Ramis, and Ilave basins, obtained using the GR4J and MGB hydrological models. Each row within the figure corresponds to a different basin and showcases the comparative performance of the models under the influence of various precipitation datasets. For each basin, we employed the observed streamflow plus the GPPs IMERG_FR, CHIRPS, SM2RAIN, and PERSIANN_CCS (for Ilave). These products were selected based on their potential to capture relevant hydrological trends and represent varying precipitation data processing methodologies (Table 1).

In the Katari Basin, the GR4J model consistently underestimates low flows across all evaluated precipitation products, resulting in flatter and less variable low flow periods. Peak flow events are also frequently underestimated. Additionally, streamflow seasonality is characterized by erratic variability,

particularly when run with SM2RAIN. This model tends to smooth out the seasonal fluctuations in streamflow more uniformly throughout the year compared to observed data.

In contrast, the MGB in the Katari basin exhibits improved sensitivity to low-magnitude events. Simulation using IMERG_FR exhibits greater fluctuations and occasionally overestimates peak flows. On the other hand, simulation using SM2RAIN_CCI offers a more accurate representation of the observed peak flows. Overall, the MGB model demonstrates a better response to variations in precipitation inputs, which is reflected in its handling of seasonal streamflow dynamics.

In the Ilave Basin, the GR4J model consistently underestimates low flows when utilizing GPPs, leading to less variable and generally flatter low flow periods. This underestimation also extends to peak flows, where the model fails to accurately simulate these events' intensity. Additionally, the seasonality of streamflow shows significant discrepancies. Notably, erratic variability is observed when simulations incorporate PERSIANN_CSS_CDR. In contrast, simulations using IMERG_FR and CHIRPS tend to more accurately capture the expected seasonal variability, although they still struggle with precise amplitude and timing.

The MGB model in the Ilave basin also underestimates low flows. For peak flows, simulations using IMERG_FR and CHIRPS provide a good representation. In contrast, simulation using PERSIANN_CSS leads to a notable overestimation of both low and peak flows, depicting actual water flow conditions misrepresentations.

In the Ramis Basin, the GR4J model underestimates low flows when processing data from GPPs. The model frequently captures peak flows' magnitude accurately but tends to overestimate them in specific years. The seasonality of streamflow is well replicated, except for the simulation using SM2RAIN_CCI.

Switching to the MGB model in the Ramis basin improves the sensitivity to low-magnitude events, introducing more fluctuations. The MGB performs well on peak flow representations, except for some overestimations when using SM2RAIN_CCI. Nonetheless, the MGB model tends to increase variability, potentially leading to an excessive representation of seasonal variations.

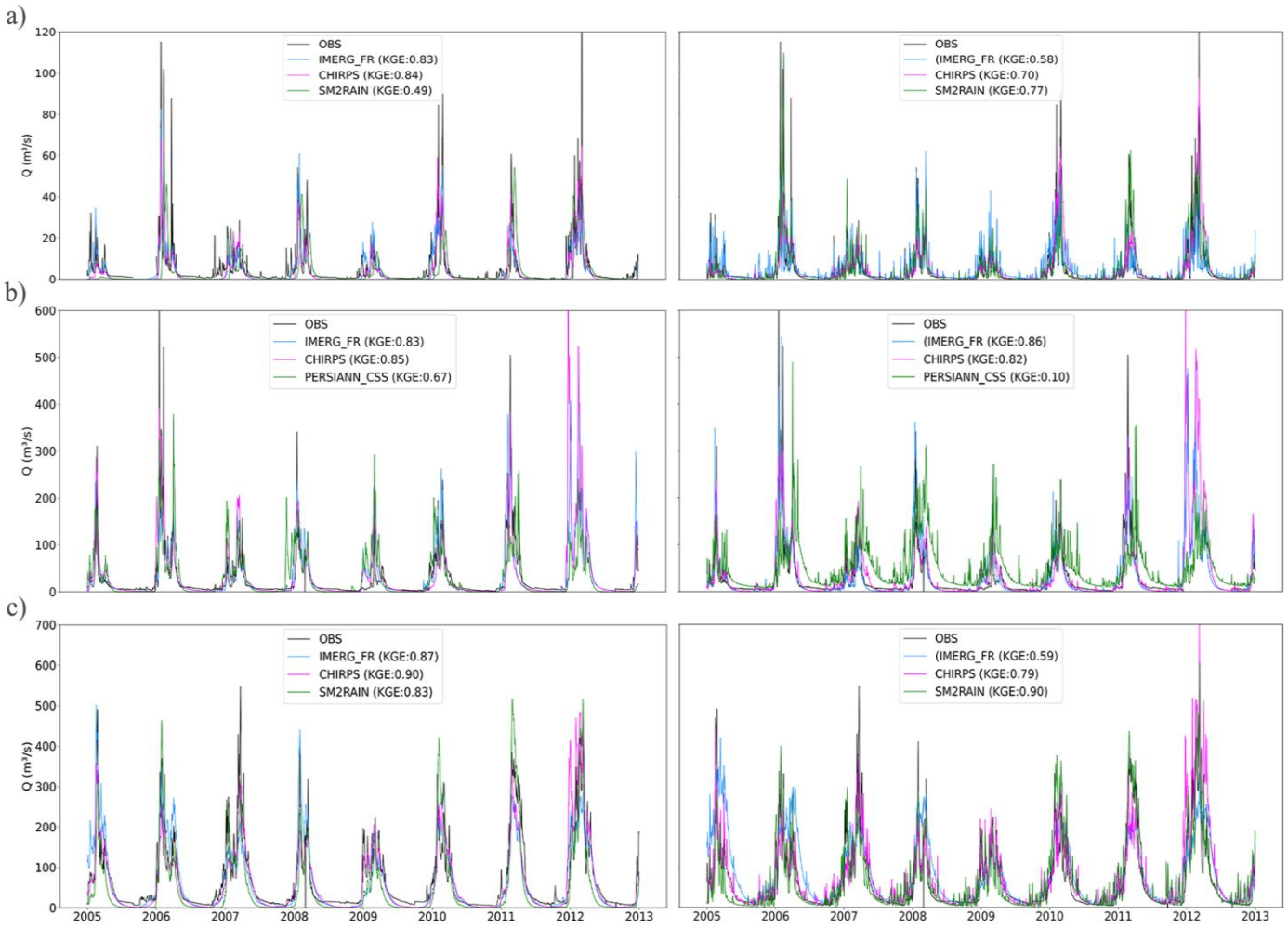

Figure 6 Comparative hydrographs of streamflow Simulations across a) Katari, b) Ilave, and c) Ramis Basins using GR4J (left) and MGB Models (right)

5. Discussion

5.1. GPP assessment in comparison to gauge observations

When addressing whether spatial resolution affects GPPs' reliability, the results show that spatial resolution may not be critical in determining accuracy. For example, PERSIANN_CSS_CDR, with the highest spatial resolution (0.04°), shows moderate correlation and significant bias, whereas MERRA2_LND, with a relatively coarse resolution (0.5°), demonstrates strong accuracy in some basins. The inclusion of gauge information tends to improve GPPs accuracy, as seen in CHIRPS, which generally shows the best performance because of additional gauge-based adjustments that are not included in CHIRP. A similar observation applies to MERRA2_LND (gauges adjusted) and _Flx (no gauges adjusted) that display distinct behaviors, with

MERRA2_LND systematically outperforming MERRA2_Flx (Reichle et al., 2011). In the case of TMPA_Adj and _RT, the gauge-based adjustment significantly decreases the bias in TMPA_Adj compared to TMPA_RT. However, the gauges' adjustment is not always relevant, as shown with IMERG and CMORPH versions´ products showing very similar performance between the non-corrected and the gauge-adjusted products.

Regarding how GPPs compare in their ability to represent spatial precipitation gradients, all GPPs (except ERA5, MERRA2_Flx, MERRA2_Lnd, PERSIANN_CDR, and PERSIANN_CSS_CDR) reveal a general pattern marked by a gradient from higher precipitation in the northeast to lower amounts in the southwest. This gradient is well supported, given that the substantial difference in rainfall in the north-eastern part of the region can be attributed to the Andes Mountains, which intercept much of the moisture coming from the Amazon region (Insel et al., 2010; Zubieta et al., 2015).

Despite seemingly representing regional precipitation patterns, SM2Rain_CCI has too many gaps (especially in the north-eastern region) due to (i) incomplete CCI soil moisture grid coverage and (ii) the inherent characteristics of the algorithms used to convert soil moisture data into precipitation estimates (Miao et al., 2023). The discrepancies in the accuracy of this product suggest the need for region-specific calibration (Satgé et al., 2020; Levizzani et al., 2020).

Compared to the state of the art, the high reliability of CHIRPS across the three basins aligns with previous research conducted in the Andean and other mountainous regions (López-Bermeo et al., 2022; Newell et al., 2023; Satgé et al., 2019), as well as in neighboring basins like the La Plata Basin (Cerón et al., 2020) and the Upper Cauca River Basin in Colombia (Romero-Hernández et al., 2024), emphasizing its effectiveness in complex topographical settings.

Furthermore, the consistent underestimation of precipitation by CMORPH_CRT in the three basins is also reflected in the study of Zubieta et al. (2015) while the poor accuracy of PERSIANN' GPPs characterized by significant overestimations in complex terrains is in line with previous studies led in Pakistan and Madagascar (Hussain et al., 2018; Ollivier et al., 2023). The overall good reliability of IMERG (ER, LR, and

FR) and MSWEP in comparison to available GPPs was also demonstrated in Brazil (Satgé et al., 2021), Madagascar (Ollivier et al., 2023), and Africa (Kouakou et al., 2023; Nwachukwu et al., 2020).

5.2. GPPs assessment in hydrological models

The ability of hydrological models to accurately simulate streamflow is heavily dependent on the accuracy and appropriateness of the input precipitation data, which must align with each basin's unique hydrological and climatological conditions (Tobin & Bennett, 2014). Variations in GPP's performance arise from discrepancies in data sources, retrieval algorithms, and the methodologies employed in bias corrections, introducing significant uncertainties in model representation of rainfall-runoff processes (Vergara et al., 2014; Zubieta et al., 2015). Additionally, the inherent uncertainties in model parameters and structure further compound these challenges, affecting the reliability of streamflow predictions, especially in arid regions where episodic low flows complicate calibration (Andrade et al., 2024).

In this context, GPP's spatial distribution should influence the performance of the hydrological models, particularly the semi-distributed MGB model, which incorporates spatial variability. In lumped models (i.e., GR4J), spatial variability is less critical, as these models rely more on the total precipitation amount and temporal distribution. However, the results indicate that spatial variability was not a decisive factor in model performance. Indeed, despite offering the highest spatial resolution, PERSIANN_CSS_CDR (0.04°) provides one of the least reliable streamflow simulations in MGB (KGE close to 0 or negative). Actually, the three most efficient GPPs for streamflow modeling in the three basins—Katari (SM2Rain_CCI 0.1°, GSMaP_Adj 0.1° and CMORPH_BLD 0.25°), Ilave (IMERG_FR 0.1°, CHIRPS 0.05°, and TMPA_Adj 0.25°), and Ramis (SM2Rain_CCI 0.1°, IMERG_LR 0.1° and MERRA_LND 0.5 °)—are not consistently those with the highest spatial resolution.

Among the considered GPPs, CHIRPS demonstrates a substantial positive impact on the performance of both hydrological models. This finding is consistent with previous literature review based on more than a hundred research articles (Du et al., 2024) and studies led across Brazil (Satgé et al., 2021) and Africa (Kouakou

et al., 2023; Satgé et al., 2019). MSWEP exhibited notably lower KGE for the MGB model in the Ramis basin, while GR4J performed very well with this GPP, surpassing the model using observed data. The high performance of MSWEP with lumped models was also highlighted in Brazil's Amazon region (Satgé et al., 2021). Likewise, ERA5, MERRA2_FLX, and PERSIANN_CSS_CDR showed a moderate impact on the performance of GR4J. In contrast, their performance with MGB was notably poor, suggesting that models like MGB may be particularly sensitive to the overestimation of rainfall (Bias>100%).

Considering the MGB model, the highest KGE values were achieved with SM2Rain_CCI in the Ramis and Katari basins. The lower KGE observed in the Ilave basin is likely due to underestimating precipitation (Bias=-74%). The results from the SM2Rain_CCI in the Ramis and Katari basins indicate that this product can provide valuable precipitation estimates that align well with observed data in specific regions and favourable local conditions for satellite soil moisture measurements (Satgé et al., 2020). Indeed, as observed by MODIS, the considered basins are mainly covered by grasslands, which have low interference on satellite soil moisture estimates used to derive precipitation estimates by SM2Rain algorithm.

5.3. Lumped vs. semi-distributed hydrological models

The analysis indicates that GPPs closely matching observed data in terms of temporal patterns and total precipitation (e.g., CHIRPS, MSWEP, and IMERG-ER, FR, LR) are likely to improve streamflow simulations in both models in the three basins. The two models' performance variability likely originates from how they conceptualize the basin's hydrological functioning. However, inaccuracies in representing precipitation intensity reflected statistically by the bias can lead to suboptimal results with MGB. At the same time, GR4J appears more resilient to such biases represented in Figure 7 (e.g., ERA5, TMPA_RT, PERSIANN_CSS_CDR, PERSIANN_CDR, and MERRA2_FLX). Given these differences in sensitivity to precipitation biases, it is important to examine the specific characteristics of the models further.

GR4J proved more effective at reproducing streamflow at the basin outlet, likely due to its simpler, lumped structure, which is less sensitive to spatial variability and intensity errors in precipitation. This

observation aligns with the "hydrological model adaptability" framework of Wang et al. (2023), who demonstrated that a conceptual lumped model (Xinanjiang) can absorb moderate systematic biases in precipitation inputs. Indeed, GR4J's conceptual design allows it to compensate for overestimations in rainfall by calibrating parameters such as the groundwater exchange coefficient (X2, Table 3)—which controls surface–groundwater exchanges—the model can buffer errors arising from excessive precipitation estimates. The high sensitivity of this parameter enables GR4J to adjust for discrepancies, thereby improving streamflow predictions even where rainfall overestimation might otherwise skew hydrological outputs (Andrade et al., 2024).

To further analyze the relationship between precipitation bias and model performance, Figure 7 presents the correlation between bias and KGE across different GPPs. This visualization highlights how MGB and GR4J respond differently to over and underestimations in precipitation, providing additional insights into their respective sensitivities to input data uncertainties. Our first observation is that despite PERSIANN_CDR, TMPA_RT, and ERA5 overestimating precipitation, the KGE remained above 0.6 for most of the basin using GR4J.

The MGB model is more sensitive to the spatial distribution of precipitation data and quantity and cannot always compensate for significant inaccuracies in precipitation inputs, as seen in Figure 7. When precipitation magnitude is well represented, with a bias close to zero, MGB successfully simulates streamflow that closely matches observed values, as seen with SM2RAIN_CCI and TMPA_Adj. Moreover, MGB exhibits greater robustness to negative biases, achieving a KGE above 0.8 in Katari (SM2RAIN_CCI), Ilave (WFDEI_GPCC, IMERG-ER, IMERG-FR, IMERG-LR, CMORPH_CRT, CMORPH_BLD), and Ramis (MERRA_LND, IMERG_ER, CMORPH_BLD, and CMORPH_CRT).

Noting that GPP biases significantly influence hydrological model performance, implementing bias correction techniques could enhance GPP applicability. For instance, statistical bias correction methods (e.g., Machine Learning-Based) have been successfully applied (Li et al., 2023). Additionally, data fusion

approaches**,** which integrate multiple GPPs with ground-based observations, could help reduce uncertainties by leveraging the strengths of different datasets (Chen et al., 2024).

The performance of the MGB model also appears to be influenced by basin size, with higher KGE values observed in larger basins. The highest KGE was obtained in the Ramis basin (14,866 km², KGE=0.9), followed by Ilave (7,720 km², KGE=0.86) and Katari (2,519 km², KGE=0.77) (Figure 5). This trend is consistent with the fact that the MGB model was specifically designed for large-scale basins, which may explain the decline in performance as basin size decreases. In large basins, spatial aggregation of precipitation data can smooth out localized discrepancies and reduce the impact of errors in rainfall distribution (Vergara et al., 2014; Satgé et al., 2021). In smaller basins, the influence of local-scale precipitation errors may be more pronounced, leading to greater discrepancies between simulated and observed streamflow. Still, GR4J reliability slightly decreased with the basin size, with the highest KGE of 0.93, 0.85, and 0.88 for the Ramis, Ilave, and Katari basins, respectively (Figure 5), in line with a previous study carried out in the Amazon region (Satgé et al., 2021).

When representing streamflow variability, MGB tends to capture rapid fluctuations in streamflow, as seen in Figure 6, whereas GR4J produces smoother hydrographs with attenuated peaks and troughs. This difference in variability may influence the KGE calculation, as higher fluctuations in MGB-simulated streamflow can introduce discrepancies in correlation, variability, and bias components, leading to lower KGE values. In contrast, GR4J's smoother representation may result in higher KGE values if it better aligns with general observed trends, even if it does not capture extreme events as effectively as MGB.

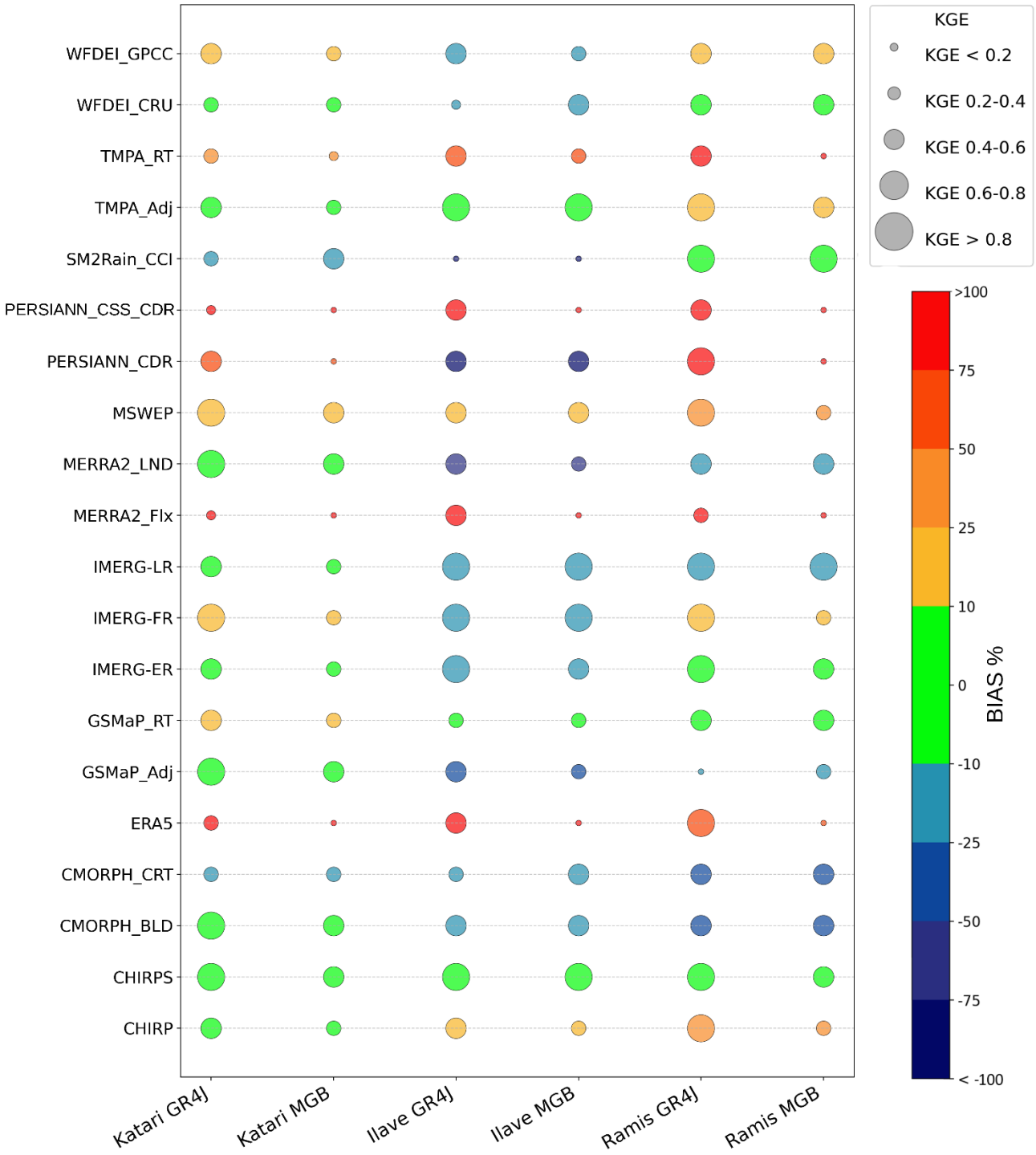

542

543 Figure 7 Bubble plot illustrating the relationship between bias and KGE for the 20 GPPs across the GR4J and MGB hydrological models in the
544 Katari, Ilave, and Ramis basins. Each bubble represents a model simulation using a given GPP, with its color indicating bias and size indicating
545 KGE.

6. Conclusions

This study evaluated the performance of 20 Gridded Precipitation Products (GPPs) at the daily time step by comparing their estimates with the one observed by the meteorological stations network and using them as input for two hydrological models—the lumped GR4J and the semi-distributed MGB. By assessing the spatial and temporal accuracy of GPPs and their impact on streamflow simulations, the study offers several key insights:

- Based on the gauge's assessment, a moderate range in GPPs reliability is observed, showing the limit of such an approach. Moreover, such assessment is subject to uncertainties related to the different spatial scales between gauges (point measurements) and GPPs (gridded observations).
- Based on the hydrological modelling assessment, the range of model performance across the 20 GPPs was substantial, with apparent differences in GPPs' reliability depending on the considered basin and hydrological model.
- Due to its lumped structure, GR4J streamflow modeling is barely influenced by precipitation bias, making it suitable for small and less complex basins. On the contrary, due to its semi-distributed structure, MGB is sensitive to precipitation bias in space and time and therefore more suitable for large and complex basins.
- The models' structure influenced high and low flow streamflow simulation with GR4J (MGB) showing greater stability in low (high) flows than MGB (GR4J).
- From an end-user perspective, GPP-driven streamflow simulations outperformed gauge-based ones in two basins, confirming their potential to mitigate the effects of sparse and uneven station networks.
- High-spatial resolution GPPs (i.e., PERSIANN_CSS_CDR) did not necessarily yield better hydrological outcomes, suggesting that spatial resolution alone is not a reliable predictor of GPP performance.

These findings contribute to a deeper understanding of how model structure interacts with precipitation uncertainty in complex, high-altitude basins. The results provide practical recommendations for selecting

GPPs and modeling strategies in transboundary and data-scarce environments. Due to the observed GPP reliability variation in space, future research should explore ensemble-based approaches that integrate multiple GPPs along with additional variables affecting precipitation dynamics in space and time (e.g., topography, cloud cover properties, vegetation, temperature, atmospheric variables) to improve precipitation monitoring across the region.

Acknowledgments

This work was supported by the Agropolis Foundation (project number: 2001-032) in the framework of the project WASACA (Wastewater irrigation: a sustainable agriculture adaptation to climate changes over the Bolivian Altiplano?). The first author is grateful to the IRD (Institut de Recherche pour le Développement) for its financial support.

7. References

Akbas, A., & Ozdemir, H. (2024). Comparing Satellite, Reanalysis, Fused and Gridded (In Situ) Precipitation Products Over Türkiye. International Journal of Climatology, 44(16), 5873-5889. https://doi.org/10.1002/joc.8671

Allan, R., Pereira, L., & Smith, M. (1998). Crop evapotranspiration-Guidelines for computing crop water requirements-FAO Irrigation and drainage paper 56 (Vol. 56).

Andrade, J. M., Ribeiro Neto, A., Nóbrega, R. L. B., Rico-Ramirez, M. A., & Montenegro, S. M. G. L. (2024). Efficiency of global precipitation datasets in tropical and subtropical catchments revealed by large sampling hydrological modelling. Journal of Hydrology, 633, 131016. https://doi.org/10.1016/j.jhydrol.2024.131016

Ashouri, H., Hsu, K.-L., Sorooshian, S., Braithwaite, D. K., Knapp, K. R., Cecil, L. D., Nelson, B. R., & Prat, O. P. (2015). PERSIANN-CDR: Daily Precipitation Climate Data Record from Multisatellite Observations for Hydrological and Climate Studies. Bulletin of the American Meteorological Society, 96(1), 69-83. https://doi.org/10.1175/BAMS-D-13-00068.1

Beck, H. E., Vergopolan, N., Pan, M., Levizzani, V., Van Dijk, A. I. J. M., Weedon, G. P., Brocca, L., Pappenberger, F., Huffman, G. J., & Wood, E. F. (2017). Global-scale evaluation of 22 precipitation datasets using gauge observations and hydrological modeling. Hydrology and Earth System Sciences, 21(12), 6201-6217. https://doi.org/10.5194/hess-21-6201-2017

Beck, H. E., Wood, E. F., Pan, M., Fisher, C. K., Miralles, D. G., Van Dijk, A. I. J. M., McVicar, T. R., & Adler, R. F. (2019). MSWEP V2 Global 3-Hourly 0.1° Precipitation: Methodology and Quantitative Assessment. Bulletin of the American Meteorological Society, 100(3), 473-500. https://doi.org/10.1175/BAMS-D-17-0138.1

Blacutt, L. A., Herdies, D. L., De Gonçalves, L. G. G., Vila, D. A., & Andrade, M. (2015). Precipitation comparison for the CFSR, MERRA, TRMM3B42 and Combined Scheme datasets in Bolivia. Atmospheric Research, 163, 117-131. https://doi.org/10.1016/j.atmosres.2015.02.002

Brêda, J. P. L. F., De Paiva, R. C. D., Collischon, W., Bravo, J. M., Siqueira, V. A., & Steinke, E. B. (2020). Climate change impacts on South American water balance from a continental-scale hydrological model driven by CMIP5 projections. Climatic Change, 159(4), 503-522. https://doi.org/10.1007/s10584-020-02667-9

Canedo, C., Pillco Zolá, R., & Berndtsson, R. (2016). Role of Hydrological Studies for the Development of the TDPS System. Water, 8(4), 144. https://doi.org/10.3390/w8040144

Cao, W., Nie, S., Ma, L., & Zhao, L. (2023). Statistical Evaluation of the Performance of Gridded Daily Precipitation Products from Reanalysis Data, Satellite Estimates, and Merged Analyses over Global Land. Remote Sensing, 15(18), 4602. https://doi.org/10.3390/rs15184602

Chen, F., Wang, Y., & Li, X. (2024). A Data- and Knowledge-Driven Method for Fusing Satellite-Derived and Ground-Based Precipitation Observations. IEEE Transactions on Geoscience and Remote Sensing, 62, 1–13. https://doi.org/10.1109/TGRS.2024.3385647

Chen, M., Huang, Y., Li, Z., Larico, A. J. M., Xue, M., Hong, Y., Hu, X.-M., Novoa, H. M., Martin, E., McPherson, R., Zhang, J., Gao, S., Wen, Y., Perez, A. V., & Morales, I. Y. (2022). Cross-Examining Precipitation Products by Rain Gauge, Remote Sensing, and WRF Simulations over a South American Region across the Pacific Coast and Andes. Atmosphere, 13(10), 1666. https://doi.org/10.3390/atmos13101666

Collischonn, W., Allasia, D., Da Silva, B. C., & Tucci, C. E. M. (2007). The MGB-IPH model for large-scale rainfall—Runoff modelling. Hydrological Sciences Journal, 52(5), 878-895. https://doi.org/10.1623/hysj.52.5.878

Collischonn, W., & Tucci, C. (2001). Simulação Hidrológica de Grandes Bacias. Revista Brasileira de Recursos Hídricos, 6(1), 95-118. https://doi.org/10.21168/rbrh.v6n1.p95-118

Dawa, S. Y., Tan, M. L., Samat, N., Roy, R., & Zhang, F. (2024). Evaluation of five gridded precipitation products for estimating precipitation and drought over Yobe, Nigeria. Water Supply, 24(6), 2039-2054. https://doi.org/10.2166/ws.2024.113

Dembélé, M., Schaefli, B., Van De Giesen, N., & Mariéthoz, G. (2020). Suitability of 17 gridded rainfall and temperature datasets for large-scale hydrological modelling in West Africa. Hydrology and Earth System Sciences, 24(11), 5379–5406. https://doi.org/10.5194/hess-24-5379-2020

De Moraes Cordeiro, A. L., & Blanco, C. J. C. (2021). Assessment of satellite products for filling rainfall data gaps in the Amazon region. Natural Resource Modeling, 34(2), e12298. https://doi.org/10.1111/nrm.12298

De Paiva, R. C. D., Buarque, D. C., Collischonn, W., Bonnet, M., Frappart, F., Calmant, S., & Bulhões Mendes, C. A. (2013). Large-scale hydrologic and hydrodynamic modeling of the Amazon River basin. Water Resources Research, 49(3), 1226-1243. https://doi.org/10.1002/wrcr.20067

Dijkshoorn, K., Huting, J., & Tempel, P. (s. f.). Update of the 1:5 million Soil and Terrain Database for Latin America and the Caribbean (SOTERLAC).

Du, H., Tan, M. L., Zhang, F., Chun, K. P., Li, L., & Kabir, M. H. (2024). Evaluating the effectiveness of CHIRPS data for hydroclimatic studies. Theoretical and Applied Climatology, 155(3), 1519-1539. https://doi.org/10.1007/s00704-023-04721-9

Fabre, J., Ruelland, D., Dezetter, A., & Grouillet, B. (2015). Accounting for hydro-climatic and water use variability in the assessment of past and future water balance at the basin scale. Proceedings of the International Association of Hydrological Sciences, 371, 43-48. https://doi.org/10.5194/piahs-371-43-2015

Faty, B., Sterk, G., Ali, A., Sy, S., Dacosta, H., Diop, S., & Descroix, L. (2023). Satellite-based rainfall estimates to simulate daily streamflow using a hydrological model over Gambia watershed. Water Science, 37(1), 151-168. https://doi.org/10.1080/23570008.2023.2225898

Fleischmann, A., Siqueira, V., Paris, A., Collischonn, W., Paiva, R., Gossett, M., Pontes, P., Calmant, S., Biancamaria, S., Crétaux, J.-F., & Tanimoune, B. (2017). Coupled hydrologic and hydraulic modeling of Upper Niger River Basin. 884. EGU General Assembly Conference Abstracts.

Friedl, M., & Sulla-Menashe, D. (2022). MODIS/Terra+Aqua Land Cover Type Yearly L3 Global 500m SIN Grid V061 [Dataset]. NASA EOSDIS Land Processes Distributed Active Archive Center. https://doi.org/10.5067/MODIS/MCD12Q1.061

Funk, C., Peterson, P., Landsfeld, M., Pedreros, D., Verdin, J., Shukla, S., Husak, G., Rowland, J., Harrison, L., Hoell, A., & Michaelsen, J. (2015). The climate hazards infrared precipitation with stations—A new environmental record for monitoring extremes. Scientific Data, 2(1), 150066. https://doi.org/10.1038/sdata.2015.66

Gao, Z., Tang, G., Jing, W., Hou, Z., Yang, J., & Sun, J. (2023). Evaluation of Multiple Satellite, Reanalysis, and Merged Precipitation Products for Hydrological Modeling in the Data-Scarce Tributaries of the Pearl River Basin, China. Remote Sensing, 15(22), 5349. https://doi.org/10.3390/rs15225349

Gebrechorkos, S. H., Leyland, J., Dadson, S. J., Cohen, S., Slater, L., Wortmann, M., Ashworth, P. J., Bennett, G. L., Boothroyd, R., Cloke, H., Delorme, P., Griffith, H., Hardy, R., Hawker, L., McLelland, S., Neal, J., Nicholas, A., Tatem, A. J., Vahidi, E., … Darby, S. E. (2024). Global-scale evaluation of precipitation datasets for hydrological modelling. Hydrology and Earth System Sciences, 28(14), 3099–3118. https://doi.org/10.5194/hess-28-3099-2024

Gelaro, R., McCarty, W., Suárez, M. J., Todling, R., Molod, A., Takacs, L., Randles, C. A., Darmenov, A., Bosilovich, M. G., Reichle, R., Wargan, K., Coy, L., Cullather, R., Draper, C., Akella, S., Buchard, V., Conaty, A., Da Silva, A. M., Gu, W., … Zhao, B. (2017). The Modern-Era Retrospective Analysis for Research and Applications, Version 2 (MERRA-2). Journal of Climate, 30(14), 5419-5454. https://doi.org/10.1175/JCLI-D-16-0758.1

Ghorbanian, A., Mohammadzadeh, A., Jamali, S., & Duan, Z. (2022). Performance Evaluation of Six Gridded Precipitation Products throughout Iran Using Ground Observations over the Last Two Decades (2000–2020). Remote Sensing, 14(15), 3783. https://doi.org/10.3390/rs14153783

Guan, X., Zhang, J., Yang, Q., Tang, X., Liu, C., Jin, J., Liu, Y., Bao, Z., & Wang, G. (2020). Evaluation of Precipitation Products by Using Multiple Hydrological Models over the Upper Yellow River Basin, China. Remote Sensing, 12(24), 4023. https://doi.org/10.3390/rs12244023

Gupta, H. V., Kling, H., Yilmaz, K. K., & Martinez, G. F. (2009). Decomposition of the mean squared error and NSE performance criteria: Implications for improving hydrological modelling. Journal of Hydrology, 377(1-2), 80-91. https://doi.org/10.1016/j.jhydrol.2009.08.003

Haghnegahdar, A., Tolson, B. A., Craig, J. R., & Paya, K. T. (2015). Assessing the performance of a semi-distributed hydrological model under various watershed discretization schemes. Hydrological Processes, 29(18), 4018-4031. https://doi.org/10.1002/hyp.10550

Hersbach, H., Bell, B., Berrisford, P., Hirahara, S., Horányi, A., Muñoz-Sabater, J., Nicolas, J., Peubey, C., Radu, R., Schepers, D., Simmons, A., Soci, C., Abdalla, S., Abellan, X., Balsamo, G., Bechtold, P., Biavati, G., Bidlot, J., Bonavita, M., … Thépaut, J. (2020). The ERA5 global reanalysis. Quarterly Journal of the Royal Meteorological Society, 146(730), 1999-2049. https://doi.org/10.1002/qj.3803

Hostache, R., Rains, D., Mallick, K., Chini, M., Pelich, R., Lievens, H., Fenicia, F., Corato, G., Verhoest, N. E. C., & Matgen, P. (2020). Assimilation of Soil Moisture and Ocean Salinity (SMOS) brightness temperature into a large-scale distributed conceptual hydrological model to improve soil moisture predictions: The Murray–Darling basin in Australia as a test case. Hydrology and Earth System Sciences, 24(10), 4793-4812. https://doi.org/10.5194/hess-24-4793-2020

Hublart, P., Ruelland, D., García De Cortázar Atauri, I., & Ibacache, A. (2015). Reliability of a conceptual hydrological model in a semi-arid Andean catchment facing water-use changes. Proceedings of the International Association of Hydrological Sciences, 371, 203-209. https://doi.org/10.5194/piahs-371-203-2015

Hublart, P., Ruelland, D., García De Cortázar-Atauri, I., Gascoin, S., Lhermitte, S., & Ibacache, A. (2016). Reliability of lumped hydrological modeling in a semi-arid mountainous catchment facing water-use changes. Hydrology and Earth System Sciences, 20(9), 3691-3717. https://doi.org/10.5194/hess-20-3691-2016

Huffman, G. J., Adler, R. F., Bolvin, D. T., & Nelkin, E. J. (2010). The TRMM Multi-Satellite Precipitation Analysis (TMPA). En M. Gebremichael & F. Hossain (Eds.), Satellite Rainfall Applications for Surface Hydrology (pp. 3-22). Springer Netherlands. https://doi.org/10.1007/978-90-481-2915-7_1

Huffman, G. J, Bolvin, D. T., Braithwaite, D., Hsu, K., Joyce, R., Kidd, C., & Xie, P. (2018). NASA global precipitation measurement (GPM) integrated multi-satellite retrievals for GPM (IMERG). Algorithm Theoretical Basis Document (ATBD). https://gpm.nasa.gov/sites/default/files/2020-05/IMERG_ATBD_V06.3.pdf

Huffman, G. J., Bolvin, D. T., Braithwaite, D., Hsu, K.-L., Joyce, R. J., Kidd, C., Nelkin, E. J., Sorooshian, S., Stocker, E. F., Tan, J., Wolff, D. B., & Xie, P. (2020a). Integrated Multi-satellite Retrievals for the Global Precipitation Measurement (GPM) Mission (IMERG). En V. Levizzani, C. Kidd, D. B. Kirschbaum, C. D. Kummerow, K. Nakamura, & F. J. Turk (Eds.), Satellite Precipitation Measurement (Vol. 67, pp. 343-353). Springer International Publishing. https://doi.org/10.1007/978-3-030-24568-9_19

Huffman, G. J., Bolvin, D. T., Braithwaite, D., Hsu, K.-L., Joyce, R. J., Kidd, C., Nelkin, E. J., Sorooshian, S., Stocker, E. F., Tan, J., Wolff, D. B., & Xie, P. (2020b). Integrated Multi-satellite Retrievals for the Global Precipitation Measurement (GPM) Mission (IMERG). En V. Levizzani, C. Kidd, D. B. Kirschbaum, C. D. Kummerow, K. Nakamura, & F. J. Turk (Eds.), Satellite Precipitation Measurement (Vol. 67, pp. 343-353). Springer International Publishing. https://doi.org/10.1007/978-3-030-24568-9_19

Hussain, Y., Satgé, F., Hussain, M. B., Martinez-Carvajal, H., Bonnet, M.-P., Cárdenas-Soto, M., Roig, H. L., & Akhter, G. (2018). Performance of CMORPH, TMPA, and PERSIANN rainfall datasets over plain, mountainous, and glacial regions of Pakistan. Theoretical and Applied Climatology, 131(3-4), 1119-1132. https://doi.org/10.1007/s00704-016-2027-z

Insel, N., Poulsen, C. J., & Ehlers, T. A. (2010). Influence of the Andes Mountains on South American moisture transport, convection, and precipitation. Climate Dynamics, 35(7-8), 1477-1492. https://doi.org/10.1007/s00382-009-0637-1

International Water Management Institute (IWMI). (2021). Data sharing in transboundary waters: Current extent, future potential and practical recommendations. International Water Management Institute (IWMI). https://doi.org/10.5337/2021.232

Jahanshahi, A., Roshun, S. H., & Booij, M. J. (2024). Comparison of satellite-based and reanalysis precipitation products for hydrological modeling over a data-scarce region. Climate Dynamics, 62(5), 3505-3537. https://doi.org/10.1007/s00382-023-07078-x

Jiang, W., Niu, Z., Wang, L., Yao, R., Gui, X., Xiang, F., & Ji, Y. (2022). Impacts of Drought and Climatic Factors on Vegetation Dynamics in the Yellow River Basin and Yangtze River Basin, China. Remote Sensing, 14(4), 930. https://doi.org/10.3390/rs14040930

Joyce, R. J., Janowiak, J. E., Arkin, P. A., & Xie, P. (2004). CMORPH: A Method that Produces Global Precipitation Estimates from Passive Microwave and Infrared Data at High Spatial and Temporal Resolution. Journal of Hydrometeorology, 5(3), 487-503. https://doi.org/10.1175/1525-7541(2004)005<0487:CAMTPG>2.0.CO;2

Kling, H., & Gupta, H. (2009). On the development of regionalization relationships for lumped watershed models: The impact of ignoring sub-basin scale variability. Journal of Hydrology, 373(3-4), 337-351. https://doi.org/10.1016/j.jhydrol.2009.04.031

Knoben, W. J. M., Freer, J. E., Fowler, K. J. A., Peel, M. C., & Woods, R. A. (2019). Modular Assessment of Rainfall–Runoff Models Toolbox (MARRMoT) v1.2: An open-source, extendable framework providing implementations of 46 conceptual hydrologic models as continuous state-space formulations. Geoscientific Model Development, 12(6), 2463-2480. https://doi.org/10.5194/gmd-12-2463-2019

Kodja, D. J., Akognongbé, A. J. S., Amoussou, E., Mahé, G., Vissin, E. W., Paturel, J.-E., & Houndénou, C. (2020). Calibration of the hydrological model GR4J from potential evapotranspiration estimates by the Penman-Monteith and Oudin methods in the Ouémé watershed (West Africa). Proceedings of the International Association of Hydrological Sciences, 383, 163-169. https://doi.org/10.5194/piahs-383-163-2020

Kouakou, C., Paturel, J.-E., Satgé, F., Tramblay, Y., Defrance, D., & Rouché, N. (2023). Comparison of gridded precipitation estimates for regional hydrological modeling in West and Central Africa. Journal of Hydrology: Regional Studies, 47, 101409. https://doi.org/10.1016/j.ejrh.2023.101409

Kubota, T., Aonashi, K., Ushio, T., Shige, S., Takayabu, Y. N., Kachi, M., Arai, Y., Tashima, T., Masaki, T., Kawamoto, N., Mega, T., Yamamoto, M. K., Hamada, A., Yamaji, M., Liu, G., & Oki, R. (2020). Global Satellite Mapping of Precipitation (GSMaP) Products in the GPM Era. En V. Levizzani, C. Kidd, D. B. Kirschbaum, C. D. Kummerow, K. Nakamura, & F. J. Turk (Eds.), Satellite Precipitation Measurement (Vol. 67, pp. 355-373). Springer International Publishing. https://doi.org/10.1007/978-3-030-24568-9_20

Levizzani, V., Kidd, C., Kirschbaum, D. B., Kummerow, C. D., Nakamura, K., & Turk, F. J. (Eds.). (2020). Satellite Precipitation Measurement: Volume 2 (Vol. 69). Springer International Publishing. https://doi.org/10.1007/978-3-030-35798-6

Li, H., Zhang, Y., Lei, H., & Hao, X. (2023). Machine Learning-Based Bias Correction of Precipitation Measurements at High Altitude. Remote Sensing, 15(8), 2180. https://doi.org/10.3390/rs15082180

Li, Y., Pang, B., Zheng, Z., Chen, H., Peng, D., Zhu, Z., & Zuo, D. (2023). Evaluation of Four Satellite Precipitation Products over Mainland China Using Spatial Correlation Analysis. Remote Sensing, 15(7), 1823. https://doi.org/10.3390/rs15071823

Liu, D. (2020). A rational performance criterion for hydrological model. Journal of Hydrology, 590, 125488. https://doi.org/10.1016/j.jhydrol.2020.125488

López-Bermeo, C., Montoya, R. D., Caro-Lopera, F. J., & Díaz-García, J. A. (2022). Validation of the accuracy of the CHIRPS precipitation dataset at representing climate variability in a tropical mountainous region of South America. Physics and Chemistry of the Earth, Parts A/B/C, 127, 103184. https://doi.org/10.1016/j.pce.2022.103184

Maggioni, V., Meyers, P. C., & Robinson, M. D. (2016). A Review of Merged High-Resolution Satellite Precipitation Product Accuracy during the Tropical Rainfall Measuring Mission (TRMM) Era. Journal of Hydrometeorology, 17(4), 1101-1117. https://doi.org/10.1175/JHM-D-15-0190.1

Martel, J.-L., Brissette, F., & Poulin, A. (2020). Impact of the spatial density of weather stations on the performance of distributed and lumped hydrological models. Canadian Water Resources Journal / Revue Canadienne Des Ressources Hydriques, 45(2), 158-171. https://doi.org/10.1080/07011784.2020.1729241

Medrano, S. C., Satgé, F., Molina-Carpio, J., Zolá, R. P., & Bonnet, M.-P. (2023). Downscaling Daily Satellite-Based Precipitation Estimates Using MODIS Cloud Optical and Microphysical Properties in Machine-Learning Models. Atmosphere, 14(9), 1349. https://doi.org/10.3390/atmos14091349

Miao, L., Wei, Z., Hu, F., & Duan, Z. (2023). Influences of Using Different Satellite Soil Moisture Products on SM2RAIN for Rainfall Estimation Across the Tibetan Plateau. IEEE Journal of Selected Topics in Applied Earth Observations and Remote Sensing, 16, 6902-6916. https://doi.org/10.1109/JSTARS.2023.3296455

Molina-Carpio, J., Rivera, I. A., Espinoza-Romero, D., Cerón, W. L., Espinoza, J., & Ronchail, J. (2023). Regionalization of rainfall in the upper Madeira basin based on interannual and decadal variability: A multi-seasonal approach. International Journal of Climatology, 43(14), 6402-6419. https://doi.org/10.1002/joc.8211

Mosaffa, H., Filippucci, P., Massari, C., Ciabatta, L., & Brocca, L. (2023). SM2RAIN-Climate, a monthly global long-term rainfall dataset for climatological studies. Scientific Data, 10(1), 749. https://doi.org/10.1038/s41597-023-02654-6

Mukuyu, P., Lautze, J., Rieu-Clarke, A., Saruchera, D., & McCartney, M. (2023). Do needs motivate the exchange of data in transboundary waters? Insights from Africa's shared basins. Water International, 48(8), 915-941. https://doi.org/10.1080/02508060.2023.2177075

Nawaz, M., Iqbal, M. F., & Mahmood, I. (2021). Validation of CHIRPS satellite-based precipitation dataset over Pakistan. Atmospheric Research, 248, 105289. https://doi.org/10.1016/j.atmosres.2020.105289

Ndiaye, P. M., Bodian, A., Dezetter, A., Ogilvie, A., & Goudiaby, O. (2024). Sensitivity of global hydrological models to potential evapotranspiration estimation methods in the Senegal River Basin (West Africa). Journal of Hydrology: Regional Studies, 53, 101823. https://doi.org/10.1016/j.ejrh.2024.101823

Newell, F., Ausprey, I. J., & Robinson, S. K. (2024). Spatiotemporal climate variability in the Andes of northern Peru: Evaluation of gridded datasets to describe cloud forest microclimate and local rainfall. https://doi.org/10.48350/182053

Nguyen, T., Masih, I., Mohamed, Y., & Van Der Zaag, P. (2018). Validating Rainfall-Runoff Modelling Using Satellite-Based and Reanalysis Precipitation Products in the Sre Pok Catchment, the Mekong River Basin. Geosciences, 8(5), 164. https://doi.org/10.3390/geosciences8050164

Nwachukwu, P. N., Satge, F., Yacoubi, S. E., Pinel, S., & Bonnet, M.-P. (2020). From TRMM to GPM: How Reliable Are Satellite-Based Precipitation Data across Nigeria? Remote Sensing, 12(23), 3964. https://doi.org/10.3390/rs12233964

Oliveira, R. F. D., Zolin, C. A., Victoria, D. D. C., Lopes, T. R., Vendrusculo, L. G., & Paulino, J. (2019). Hydrological calibration and validation of the MGB-IPH model for water resource management in the upper Teles Pires River basin in the Amazon-Cerrado ecotone in Brazil. Acta Amazonica, 49(1), 54-63. https://doi.org/10.1590/1809-4392201800812

Ollivier, C. C., Carrière, S. D., Heath, T., Olioso, A., Rabefitia, Z., Rakoto, H., Oudin, L., & Satgé, F. (2023). Ensemble precipitation estimates based on an assessment of 21 gridded precipitation datasets to improve precipitation estimations across Madagascar. Journal of Hydrology: Regional Studies, 47, 101400. https://doi.org/10.1016/j.ejrh.2023.101400

Paiva, R. C. D., Collischonn, W., & Tucci, C. E. M. (2011). Large scale hydrologic and hydrodynamic modeling using limited data and a GIS based approach. Journal of Hydrology, 406(3-4), 170-181. https://doi.org/10.1016/j.jhydrol.2011.06.007

Perrin, C., Michel, C., & Andréassian, V. (2003). Improvement of a parsimonious model for streamflow simulation. Journal of Hydrology, 279(1-4), 275-289. https://doi.org/10.1016/S0022-1694(03)00225-7

Pillco Zolá, R., Bengtsson, L., Berndtsson, R., Martí-Cardona, B., Satgé, F., Timouk, F., Bonnet, M.-P., Mollericon, L., Gamarra, C., & Pasapera, J. (2019). Modelling Lake Titicaca's daily and monthly evaporation. Hydrology and Earth System Sciences, 23(2), 657-668. https://doi.org/10.5194/hess-23-657-2019

Pontes, P. R. M., Fan, F. M., Fleischmann, A. S., de Paiva, R. C. D., Buarque, D. C., Siqueira, V. A., Jardim, P. F., Sorribas, M. V., & Collischonn, W. (2017). MGB-IPH model for hydrological and hydraulic simulation of large floodplain river systems coupled with open source GIS. Environmental Modelling & Software, 94, 1-20. https://doi.org/10.1016/j.envsoft.2017.03.029

Pozo Valdivieso. (2024). SIMULACIÓN DE ESCENARIOS FUTUROS DE DISPONIBILIDAD DE AGUA EN BASE A SITUACIONES CLIMÁTICAS EXTREMAS OBSERVADAS EN EL PASADO [Escuela Politecnica Nacional]. http://bibdigital.epn.edu.ec/handle/15000/25696

Prat, O. P., Nelson, B. R., Nickl, E., & Leeper, R. D. (2021). Global evaluation of gridded satellite precipitation products from the NOAA Climate Data Record program. Journal of Hydrometeorology. https://doi.org/10.1175/JHM-D-20-0246.1

Quispe, L. A., Paxi, E., & Lujano, E. (2023). Evaluation of GPM IMERG Performance Over the Lake Titicaca Basin at Different Time Scales. ECWS-7 2023, 65. https://doi.org/10.3390/ECWS-7-14324

Raimonet, M., Oudin, L., Thieu, V., Silvestre, M., Vautard, R., Rabouille, C., & Le Moigne, P. (2017). Evaluation of Gridded Meteorological Datasets for Hydrological Modeling. Journal of Hydrometeorology, 18(11), 3027-3041. https://doi.org/10.1175/JHM-D-17-0018.1

Rao, P., Wang, F., Yuan, X., Liu, Y., & Jiao, Y. (2024). Evaluation and comparison of 11 sets of gridded precipitation products over the Qinghai-Tibet Plateau. Atmospheric Research, 302, 107315. https://doi.org/10.1016/j.atmosres.2024.107315

Reichle, R. H., Koster, R. D., De Lannoy, G. J. M., Forman, B. A., Liu, Q., Mahanama, S. P. P., & Touré, A. (2011). Assessment and Enhancement of MERRA Land Surface Hydrology Estimates. Journal of Climate, 24(24), 6322-6338. https://doi.org/10.1175/JCLI-D-10-05033.1

Roche, M. A., Bourges, J., Cortes, J., & Mattos, R. (1992). Climatology And Hydrology. En C. Dejoux & A. Iltis (Eds.), Lake Titicaca (Vol. 68, pp. 63-88). Springer Netherlands. https://doi.org/10.1007/978-94-011-2406-5_4

Romero-Hernández, C. M., Avila-Diaz, A., Quesada, B., Medeiros, F., Cerón, W. L., Guzman-Escalante, J., Ocampo-Marulanda, C., Rodrigues Torres, R., & Zuluaga, C. F. (2024). Bias-corrected high-resolution precipitation datasets assessment over a tropical mountainous region in Colombia: A case of study in Upper Cauca River Basin. Journal of South American Earth Sciences, 140, 104898. https://doi.org/10.1016/j.jsames.2024.104898

Ruelland, D., Dezetter, A., & Hublart, P. (s. f.). Sensitivity analysis of hydrological modelling to climate forcing in a semi-arid mountainous catchment.

Sadeghi, M., Nguyen, P., Naeini, M. R., Hsu, K., Braithwaite, D., & Sorooshian, S. (2021). PERSIANN-CCS-CDR, a 3-hourly 0.04° global precipitation climate data record for heavy precipitation studies. Scientific Data, 8(1), 157. https://doi.org/10.1038/s41597-021-00940-9

Sahu, M. K., Shwetha, H. R., & Dwarakish, G. S. (2023). State-of-the-art hydrological models and application of the HEC-HMS model: A review. Modeling Earth Systems and Environment, 9(3), 3029-3051. https://doi.org/10.1007/s40808-023-01704-7

Satgé, F., Defrance, D., Sultan, B., Bonnet, M.-P., Seyler, F., Rouché, N., Pierron, F., & Paturel, J.-E. (2020). Evaluation of 23 gridded precipitation datasets across West Africa. Journal of Hydrology, 581, 124412. https://doi.org/10.1016/j.jhydrol.2019.124412

Satgé, F., Pillot, B., Roig, H., & Bonnet, M.-P. (2021). Are gridded precipitation datasets a good option for streamflow simulation across the Juruá river basin, Amazon? Journal of Hydrology, 602, 126773. https://doi.org/10.1016/j.jhydrol.2021.126773

Satgé, F., Ruelland, D., Bonnet, M.-P., Molina, J., & Pillco, R. (2019). Consistency of satellite-based precipitation products in space and over time compared with gauge observations and snow- hydrological modelling in the Lake Titicaca region. Hydrology and Earth System Sciences, 23(1), 595-619. https://doi.org/10.5194/hess-23-595-2019

Scheel, M. L. M., Rohrer, M., Huggel, Ch., Santos Villar, D., Silvestre, E., & Huffman, G. J. (2011). Evaluation of TRMM Multi-satellite Precipitation Analysis (TMPA) performance in the Central Andes region and its dependency on spatial and temporal resolution. Hydrology and Earth System Sciences, 15(8), 2649-2663. https://doi.org/10.5194/hess-15-2649-2011

Shiru, M. S., Chung, E.-S., & Sa'adi, Z. (2025). Performance Assessment of Satellite Precipitation Products over Nigeria: A Compromise Programming Approach. Earth Systems and Environment. https://doi.org/10.1007/s41748-024-00563-1

Singh, A. K., & Singh, V. (2024). Assessing the accuracy and reliability of satellite-derived precipitation products in the Kosi River basin (India). Environmental Monitoring and Assessment, 196(7), 671. https://doi.org/10.1007/s10661-024-12785-x

Siqueira, V. A., Paiva, R. C. D., Fleischmann, A. S., Fan, F. M., Ruhoff, A. L., Pontes, P. R. M., Paris, A., Calmant, S., & Collischonn, W. (2018). Toward continental hydrologic–hydrodynamic modeling in South America. Hydrology and Earth System Sciences, 22(9), 4815-4842. https://doi.org/10.5194/hess-22-4815-2018

Siqueira, V., Fleischmann, A., Jardim, P., Fan, F., & Collischonn, W. (2016). IPH-Hydro Tools: A GIS coupled tool for watershed topology acquisition in an open-source environment. Revista Brasileira de Recursos Hídricos, 21(1), 274-287. https://doi.org/10.21168/rbrh.v21n1.p274-287

Sun, Q., Miao, C., Duan, Q., Ashouri, H., Sorooshian, S., & Hsu, K. (2018). A Review of Global Precipitation Data Sets: Data Sources, Estimation, and Intercomparisons. Reviews of Geophysics, 56(1), 79-107. https://doi.org/10.1002/2017RG000574

Tan, M. L., Gassman, P. W., Srinivasan, R., Arnold, J. G., & Yang, X. (2019). A Review of SWAT Studies in Southeast Asia: Applications, Challenges and Future Directions. Water, 11(5), 914. https://doi.org/10.3390/w11050914

Taylor, K. E. (2001). Summarizing multiple aspects of model performance in a single diagram. Journal of Geophysical Research: Atmospheres, 106(D7), 7183-7192. https://doi.org/10.1029/2000JD900719

Ter Horst, R., Srinivasan, V., Wheeler, K., Timmerman, J., & Van Der Zaag, P. (2023). Exploring the use of data and models in transboundary water governance. Water International, 48(8), 909-914. https://doi.org/10.1080/02508060.2024.2304975

Tobin, K. J., & Bennett, M. E. (2014). Satellite precipitation products and hydrologic applications. Water International, 39(3), 360-380. https://doi.org/10.1080/02508060.2013.870423

Todini, E. (1996). The ARNO rainfall—Runoff model. Journal of Hydrology, 175(1-4), 339-382. https://doi.org/10.1016/S0022-1694(96)80016-3

Torres-Batlló, J., & Martí-Cardona, B. (2020). Precipitation trends over the southern Andean Altiplano from 1981 to 2018. Journal of Hydrology, 590, 125485. https://doi.org/10.1016/j.jhydrol.2020.125485

UNESCO. (2003). Cooperación sobre el lago titicaca. UNESCO. https://unesdoc.unesco.org/ark:/48223/pf0000153200_spa

Ushio, T., Sasashige, K., Kubota, T., Shige, S., Okamoto, K., Aonashi, K., Inoue, T., Takahashi, N., Iguchi, T., Kachi, M., Oki, R., Morimoto, T., & Kawasaki, Z.-I. (2009). A Kalman Filter Approach to the Global Satellite Mapping of Precipitation (GSMaP) from Combined Passive Microwave and Infrared Radiometric Data. Journal of the Meteorological Society of Japan. Ser. II, 87A, 137-151. https://doi.org/10.2151/jmsj.87A.137

Vergara, H., Hong, Y., Gourley, J. J., Anagnostou, E. N., Maggioni, V., Stampoulis, D., & Kirstetter, P.-E. (2014). Effects of Resolution of Satellite-Based Rainfall Estimates on Hydrologic Modeling Skill at Different Scales. Journal of Hydrometeorology, 15(2), 593-613. https://doi.org/10.1175/JHM-D-12-0113.1

Wan, Y., Li, D., Sun, J., Wang, M., & Liu, H. (2025). Evaluation of six latest precipitation datasets for extreme precipitation estimates and hydrological application across various climate regions in China. Atmospheric Research, 315, 107932. https://doi.org/10.1016/j.atmosres.2025.107932

Wang, J., Zhuo, L., Han, D., Liu, Y., & Rico-Ramirez, M. A. (2023). Hydrological Model Adaptability to Rainfall Inputs of Varied Quality. Water Resources Research, 59(2), e2022WR032484. https://doi.org/10.1029/2022WR032484

Wang, Z., Zhong, R., Lai, C., & Chen, J. (2017). Evaluation of the GPM IMERG satellite-based precipitation products and the hydrological utility. Atmospheric Research, 196, 151-163. https://doi.org/10.1016/j.atmosres.2017.06.020

Weedon, G. P., Balsamo, G., Bellouin, N., Gomes, S., Best, M. J., & Viterbo, P. (2014). The WFDEI meteorological forcing data set: WATCH Forcing Data methodology applied to ERA-Interim reanalysis data. Water Resources Research, 50(9), 7505-7514. https://doi.org/10.1002/2014WR015638

Wei, X., Guo, S., & Xiong, L. (2021). Improving Efficiency of Hydrological Prediction Based on Meteorological Classification: A Case Study of GR4J Model. Water, 13(18), 2546. https://doi.org/10.3390/w13182546

Xu, H., Xu, C.-Y., Sælthun, N. R., Zhou, B., & Xu, Y. (2015). Evaluation of reanalysis and satellite-based precipitation datasets in driving hydrological models in a humid region of Southern China. Stochastic Environmental Research and Risk Assessment, 29(8), 2003-2020. https://doi.org/10.1007/s00477-014-1007-z

Yamazaki, D., Ikeshima, D., Sosa, J., Bates, P. D., Allen, G. H., & Pavelsky, T. M. (2019). MERIT Hydro: A High-Resolution Global Hydrography Map Based on Latest Topography Dataset. Water Resources Research, 55(6), 5053-5073. https://doi.org/10.1029/2019WR024873

Yılmaz, M. (2025). Performance of various gridded precipitation and temperature products against gauged observations over Turkey. Earth Science Informatics, 18(1), 9. https://doi.org/10.1007/s12145-024-01512-2

Zubieta, R., Getirana, A., Espinoza, J. C., & Lavado, W. (2015). Impacts of satellite-based precipitation datasets on rainfall–runoff modeling of the Western Amazon basin of Peru and Ecuador. Journal of Hydrology, 528, 599-612. https://doi.org/10.1016/j.jhydrol.2015.06.064

Zubieta, R., Molina-Carpio, J., Laqui, W., Sulca, J., & Ilbay, M. (2021). Comparative Analysis of Climate Change Impacts on Meteorological, Hydrological, and Agricultural Droughts in the Lake Titicaca Basin. Water, 13(2), 175. https://doi.org/10.3390/w13020175